








# Shot-noise reduction for lattice Hamiltonians

Timo Eckstein <sup>1,2,\*</sup> Refik Mansuroglu <sup>1,3</sup> Stefan Wolf <sup>1</sup> Ludwig Nützel <sup>1</sup>  
Stephan Tasler <sup>1</sup> Martin Kliesch <sup>4</sup> and Michael J. Hartmann <sup>1,2</sup>

<sup>1</sup>*Department of Physics, Friedrich-Alexander Universität Erlangen-Nürnberg, Erlangen, Germany*

<sup>2</sup>*Max-Planck Institute for the Science of Light, Erlangen, Germany*

<sup>3</sup>*University of Vienna, Faculty of Physics, Boltzmannngasse 5, 1090 Wien, Austria*

<sup>4</sup>*Institute for Quantum Inspired and Quantum Optimization, Hamburg University of Technology, Germany*

Efficiently estimating energy expectation values of lattice Hamiltonians on quantum computers is a serious challenge, where established techniques can require excessive sample numbers. Here we introduce geometric partitioning as a scalable alternative. It splits the Hamiltonian into subsystems that extend over multiple lattice sites, and for which transformations between their local eigenbasis and the computational basis can be efficiently found. This allows us to reduce the number of measurements as we sample from a more concentrated distribution without diagonalizing the problem. For systems in an energy eigenstate, we prove a lower bound on the sampling number improvement over the "naive" mutually commuting local operator grouping, which grows with the considered subsystem size, consistently showing an advantage for our geometric partitioning strategy. Notably, our lower bounds do not decrease but increase for more correlated states (Theorem 1). For states that are weakly isotropically perturbed around an eigenstate, we show how the sampling number improvement translates to imperfect eigenstate improvements, namely measuring close to the true eigenbasis already for smaller perturbations (Theorem 2). We illustrate our findings on multiple two-dimensional lattice models including the transverse field XY- and Ising model as well as the Fermi Hubbard model.

## I. INTRODUCTION

Extracting information from a quantum computer means sampling from a probability distribution defined by the sampled quantum state and the observable to be measured. Since the speed of individual gate and read-out operations is for quantum computers rather low, the efficiency of a quantum algorithm or quantum simulation is often limited by the number of measurements and hence executions, that need to be made to obtain enough samples. Therefore, reducing the sampling complexity in obtaining the output of a quantum computer is a goal of utmost importance.

Specifically, measuring an observable  $O$  on a quantum state  $|\psi\rangle$  means randomly drawing the eigenvalues  $o_m$  of  $O$  with probabilities defined by the amplitudes' squares  $|c_i|^2$  of the expansion  $|\psi\rangle = \sum_i c_i |o_i\rangle$  in the eigenbasis  $\{|o_i\rangle\}$  of  $O$ . The empirical mean estimator  $\bar{O}_M := 1/M \sum_{m=1}^M o_m$  from i.i.d.  $M$  repetitions (or samples) then yields an approximation to the expectation value  $\langle O \rangle = \langle \psi | O | \psi \rangle$  with a standard error  $\sigma_O$  given by

$$\sigma_O^2 = \text{Var}(\bar{O}_M) = \frac{1}{M} \text{Var}_{|\psi\rangle}(O), \quad (1)$$

This variance of  $\bar{O}_M$  allows to quantify finite sampling noise since Chebyshev's inequality upper bounds the probability to be more than a threshold  $\epsilon$  away from the true expectation value:

$$P(|\bar{O}_M - \langle O \rangle| \geq \epsilon) \leq \text{Var}(\bar{O}_M) / \epsilon^2 \quad (2)$$

Although this is all undergraduate physics, efficient measurements in quantum computation are a very active field of research [1-3]. The reason is that measurements in quantum computation can typically only be done in a specific basis, conventionally the Pauli  $Z$  (or computational) basis. As a consequence, measuring an observable  $O$ , that is not diagonal in the computational basis, in general, requires a diagonalization  $U_M O U_M^\dagger$ , which is equivalent to implementing a rotation  $U_M$  at the end of the quantum circuit, compare Fig. 1. In general, this is however a non-trivial task, as finding and implementing the basis transformation  $U_M$ , that transforms the eigenbasis of  $O$  into the computational basis, can be as hard as solving the quantum computational problem in the first place. For instance, an energy measurement as part of a groundstate preparation cannot be performed in the energy eigenbasis, since the ability to implement  $U_M$  and its reverse would imply that any eigenstate can be prepared, thus rendering the groundstate preparation algorithm obsolete.

If the eigenbasis of  $O$  is not known, it is possible to measure parts  $O_b$ , whose eigenbases are known and that constitute the observable  $O = \sum_b O_b$ . The linearity of the expectation value then allows to estimate  $\langle O \rangle = \sum_b \langle O_b \rangle$ . Calling the set  $\mathcal{B} = \{O_1, O_2, \dots\}$  a *partition* of  $O$ , the variance of such a partitioned observable is the sum of the variances of the individual parts, so that

$$\sum_{O_b \in \mathcal{B}} \sigma_{O_b}^2 = \sum_{O_b \in \mathcal{B}} \frac{\text{Var}_{|\psi\rangle}(O_b)}{M_b} \quad (3)$$

with the overall number of measurements  $M = \sum_b M_b$  and  $M_b$  being the number of measurements for each  $O_b$ . The standard way of decomposing  $O$  into measurable parts  $O_b$  is to partition the Pauli-strings in  $O$  into mutually commuting groups of Pauli sums (compare also Fig. 1).

\* [Timo.Eckstein@fau.de](mailto:Timo.Eckstein@fau.de)

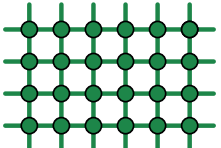
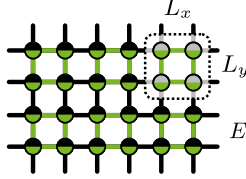
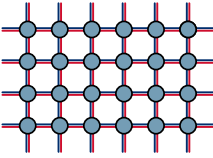
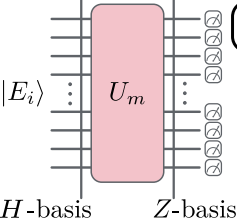
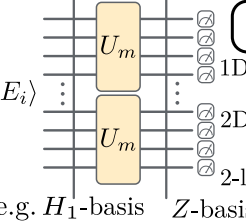
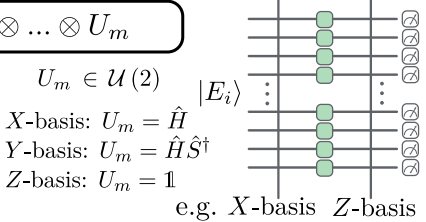
| $\mathcal{B}$              | Eigenbasis   | Geometric partitioning (Example)   | Pauli partitioning (Example)   |
|----------------------------|--|--|--|
| Graphical splitting        |  <p> <math>\circ \triangleq</math> qubit/vertex<br/> <math>\text{---} \triangleq</math> coupling/edge<br/> <math>\bullet \triangleq H</math><br/> <math>E_i = \langle E_i   H   E_i \rangle</math> </p> |  <p> <math>\text{---} \triangleq H_1</math><br/> <math>\text{---} \triangleq H_2</math><br/> <math>E_i = \langle E_i   H_1   E_i \rangle + \langle E_i   H_2   E_i \rangle</math> </p>  |  <p> <math>\text{+} \triangleq H_1</math> <math>\text{+} \triangleq H_2</math><br/> <math>\bullet \triangleq H_3</math><br/> <math>E_i = \langle E_i   H_1   E_i \rangle + \langle E_i   H_2   E_i \rangle + \langle E_i   H_3   E_i \rangle</math> </p>              |
| Measurement implementation |  <p> <math>U_M = U_m</math><br/> <math>U_m \in \mathcal{U}(2^n)</math><br/> <i>H</i>-basis      <i>Z</i>-basis </p>   |  <p> <math>U_M = U_m \otimes \dots \otimes U_m</math><br/>         1D cuts: <math>U_m \in \mathcal{U}(2^{L\sqrt{n}})</math><br/>         2D cuts: <math>U_m \in \mathcal{U}(2^{L_x \cdot L_y})</math><br/>         2-local: <math>U_m \in \mathcal{U}(2^2)</math><br/>         e.g. <i>H</i><sub>1</sub>-basis      <i>Z</i>-basis </p> |  <p> <math>U_m \in \mathcal{U}(2)</math><br/> <i>X</i>-basis: <math>U_m = \hat{H}</math><br/> <i>Y</i>-basis: <math>U_m = \hat{H} \hat{S}^\dagger</math><br/> <i>Z</i>-basis: <math>U_m = \mathbb{1}</math><br/>         e.g. <i>X</i>-basis      <i>Z</i>-basis </p> |
| Main results               | <p><b>Theorem 1: Geometric partitioning always requires less measurements than Pauli partitioning for the same sampling noise error</b></p> <p><b>Theorem 2: Sampling complexity improvements carry over to imperfect eigenstates.</b></p>   |  |  |

FIG. 1. **Concept of geometric partitioning.** To estimate the expectation value of an observable  $O$  w.r.t. a state  $|\psi\rangle$ , one would ideally want to measure  $O$  at once, meaning in its eigenbasis (first column). If this is not feasible,  $O$  must be partitioned into individually measurable parts  $O_b$  (first row), which increases the measurement error upper bound Eq. (7). For non-diagonal lattice Hamiltonians, on which we focus here, we have measuring in the eigenbasis (first column) and measuring in Pauli bases (third column), as extreme cases. For the first, the measurement error is minimal (even 0 for perfect eigenstates), but the basis transformation corresponds to a full diagonalization of  $H$ , for which the circuit is typically unknown (second row). On the other hand, the basis transformation  $U_M$  from local Pauli bases to  $Z$ -basis can be implemented efficiently with constant depth circuits, at the cost of a significantly larger measurement error. Here, we explore the intersection of these extremes, namely, measurement bases closer to the eigenbasis, that are constructed via the eigenbases of disjoint subsystems of  $H$  (second column). These naturally take the local structure of the observable  $H$  into account but the basis transformations  $U_M$  remain scalably implementable due to their block diagonal structure (second row). As our main analytical results we show in Theorem. 1 that these geometric partitionings of  $H$  always lead to less measurements for estimating  $E_i$  from  $|E_i\rangle$  compared to the Pauli partitioning baseline for the same measurement uncertainty. Further, these sampling improvements carry over to imperfect eigenstates in the form of smaller perturbation thresholds above which measuring in the geometric bases is up to a factor 2 as good as measuring in the eigenbasis (Sec. II C) (third row). We illustrate our findings with a variety of examples in Sec. II D and Sec. II E.

The challenge of reducing shot counts has received much attention in the context of applications in quantum chemistry. On the one hand, Pauli grouping methods [4–8] aim to reduce the number of  $O_b$ 's. Classical shadows [9–13], on the other hand, aim at estimating expectation values in an observable-independent fashion. This means one is not restricted to knowing a priori a specific observable of interest  $O$ , but also does not adapt the sampling strategy to the  $\text{Var}_{|\psi\rangle}(O_b)$ . Instead one aims to reduce the number of partitions  $O_b$  by restricting and using the locality of the to-be-estimated observables so that local random measurements suffice to reduce the measurement effort [8, 14]. While the Hamiltonians from quantum chemistry applications have a complex non-local interaction structure quantum spin lattices are much simpler in this regard and grouping methods only have little effect on the measurement count. Hence, different strategies are required for obtaining significant improvements in the required number of measurements for lattice systems, such as clever ways to minimize the variance terms in Eq. (3). This challenge received relatively little attention, so far.

In this work, we develop such tailored measurement schemes that make use of the lattice structure. More specifically, we reduce the  $\text{Var}_{|\psi\rangle}(O_b)$ -terms by taking advantage of lattice symmetries. While keeping much of our analysis general, we focus on translation invariant Hamiltonians  $H$  with nearest-neighbor interactions on a rectangular lattice, as can be found in numerous quantum many-body Hamiltonians, like the Ising or the Hubbard models:

$$H = \sum_{i,\alpha} h_i^{(\alpha)} o_i^{(\alpha)} + \sum_{\langle i,j \rangle, \alpha, \beta} J_{i,j}^{(\alpha,\beta)} o_i^{(\alpha)} o_j^{(\beta)} \quad (4)$$

Here, the Latin indices label lattice sites, and Greek indices single operators  $o_i$  on individual lattice sites. These can be Pauli operators  $o_i^{(\alpha)} \in \{\mathbb{1}, X, Y, Z\}$  for two-level bosonic models, or creation, annihilation and number operators in Fock space representation  $o_i^{(\alpha)} \in \{c_{i,\alpha}^\dagger, c_{i,\alpha}, n_{i,\alpha}\}$  for fermionic lattice models. The coefficients,  $h_i^{(\alpha)}$  and  $J_{i,j}^{(\alpha,\beta)}$  are real-valued coupling constants, which are conventionally labeled  $U$  and  $t$  for the (fermionic) Hubbard model. This type of Hamiltonians are of fundamental im-

portance to condensed matter physics and can be natively explored on solid-state quantum computing platforms, e.g. devices based on semiconductor spin qubits [15, 16], or superconducting circuits [17, 18], as their connectivity graph is fixed by the manufacturing and their two-qubit operations are only available on nearest neighbors. Nonetheless, our results straight-forwardly generalize to other interaction graphs, such as next-nearest neighbor interactions and bilayer graphs.

The main idea we pursue for realizing sampling improvement is to partition the geometrically local Hamiltonian  $H$  into terms  $H_b$ , which further decompose into subsystems  $H_{b,k}$  of disjoint support,  $H_b = \sum_{k=1}^K H_{b,k}$ . The transformations of the measurement bases, from the eigenbases of the  $H_{b,k}$  into the computational basis, thus become direct products  $U_M^{(H_b)} = U_{b,1} \otimes \dots \otimes U_{b,K}$  (see also Fig. 1). We call this a geometric partitioning. It becomes particularly useful if the support of the individual  $H_{b,k}$  grows such that correlations of longer and longer range can be captured well. Yet, an implementation of this measurement strategy requires that the transformations  $U_{b,k}$  are known and can be implemented. Thus, this partitioning strategy is worst case limited to patch sizes  $L_x \times L_y$ , for which diagonalization is classically tractable and the gate sequences to implement the  $U_{b,k} \in \mathcal{U}(2^{L_x \times L_y})$  can be obtained. The patches thus do not scale in the total system size. As a consequence, the circuit depth of the  $U_{b,k}$  is also constant w.r.t. the overall system size  $n$ . For translationally invariant systems all  $U_{b,k} = U_m$  will be the same so that one needs to find only once such a subsystem diagonalization circuit. For specific diagonalizable 1D lattice models, like the transverse field Ising model, exact linear depth circuits to implement  $U_m$  are known [19] and can thus be used for partitionings via 1D cuts.

We compare sample numbers  $M$  for different geometric partitions with the "standard" partition into groups of mutually commuting local operators ( $o_i^{(\alpha)}$  and  $o_i^{(\alpha)} o_j^{(\beta)}$  in Eq. (4)) under the condition of admitting the same standard error (compare Eq. (3)). Throughout this work we call the "standard" partitioning interchangeably Pauli partitioning as both often coincide for simple spin models and also fermionic lattice models under Jordan-Wigner transformation. Within our first main result (Theorem 1) we show that, for systems in an energy eigenstate, geometric partitions always outperform Pauli partitions in terms of the required sample number for eigenenergy estimation of lattice models. For example,  $5 \times 5$  subsystem patches are guaranteed to reduce  $M$  compared to Pauli partitioning by at least a factor 10. Further, we obtain lower bounds for the improvement factors of the relative measurement effort for two- and one-dimensional cuts, which can even become arbitrarily large diverge for strongly correlated states (e.g. compare Eq. (28), Example in Sec. IID 1 and Fig. 3 (a)). These cases do not require a common eigenbasis of  $H_1$  and  $H_2$  (or  $H$  and  $H_1$  or  $H_2$ ) and thus do not correspond to cases where the transformations  $U_{b,k}$  would (approximately) diagonalize  $H$ .

In Sec. IIC, we generalize the statement by integrating over fixed sized vicinities around an eigenstate to take imperfections in the state preparation on real quantum hardware into account. The result is summarized in Theorem 2, where we show how sampling improvements translate from perfect to imperfect eigenstates. We find that the transition to a regime, where sampling in the respective partitioned bases requires maximally twice as many measurements as measuring in the eigenbasis, happens for geometric partitioning significantly earlier than for Pauli partitioning. By how much is determined by the perfect eigenstate improvements that are lower bounded by Theorem 1.

In Sec. IID we numerically explore the bounds presented in Theorem 1. To show that the lower bounds we derived can be significantly exceeded, we provide in total six two-dimensional examples. These are the XY-model with a transversal Z-field (TFXYM), a special case of it the Hard-core Bose-Hubbard Model (HCBH), the Transverse field Ising model (TFIM), the Transverse field Biaxial Next nearest neighbor Ising model (TF-BNNNI), and the spinless and spinfull Hubbard model. For the TFXYM the sampling improvement becomes as large as  $\gtrsim 10^7$  around the phase boundary. For the TFIM when the 1-local field strength dominates we reobtain the improvement lower bound (Eq. (28)) indicating their tightness, whereas when the 2-local terms dominate we find improvements even scaling quadratically with its coupling (Lemma 5). The TF-BNNNI model showcases how geometric partitioning works beyond nearest-neighbor coupling, where the splittings are similar to axial 3-local models. The Hubbard model, which is 2-local in the Fock basis, depicts not only a fermionic example, but also a bilayer lattice from couplings of the spin-up and the spin-down sector. Across these examples, we find typical improvements in the range of 10 to 1000, and noticeably consistently with Theorem 1 a diverging improvement close to the TFXYM phase transition (Fig. 3 (a)).

Eventually, in Sec. IIE, analogously to the perfect eigenstates results, we provide numerical illustrations for the imperfect eigenstates results in Sec. IIC, where we focus on numerically testing our approximations and truncations.

## II. RESULTS

### A. Sampling improvement cost function

In this work, we want to use a quantitative measure to compare a measurement strategy  $\mathcal{B}_1$  that splits  $H = \sum_{H_b \in \mathcal{B}_1} H_b$  with another one  $\mathcal{B}_2$  that splits  $H = \sum_{H_b \in \mathcal{B}_2} H_b$  by determining which one requires less measurements for achieving the same standard error according to Eq. (3). Our results can also be interpreted as quantifying which strategy leads to a smaller standard error for the same number of measurements  $M$ . To achieve this, the issue we first need to resolve is that the stan-

dard error of a partitioned observable in Eq. (3), not only depends on the different partitionings but also on the specific measurement budget allocation  $M_b$ . It turns out, that comparing partitioning strategies for the optimal measurement budget allocation, which minimizes the sampling error, makes the comparison independent of the distribution of the  $M_b$  [14]:

**Lemma 1** (Optimal sampling budget allocation of partitioned observables). Let  $\mathcal{B}$  be a partitioning of the observable  $H = \sum_{H_b \in \mathcal{B}} H_b$ , then the standard error of the partitioned observable under optimal allocation of sampling budget  $M = \sum M_b$  is given by:

$$\begin{aligned} \sigma_{\mathcal{B}}^2 &= \min_{M=\sum M_b} \left( \sum_{H_b \in \mathcal{B}} \frac{\text{Var}_{|\psi\rangle}(H_b)}{M_b} \right) \\ &= \frac{1}{M} \left[ \sum_{H_b \in \mathcal{B}} \sqrt{\text{Var}_{|\psi\rangle}(H_b)} \right]^2 \end{aligned} \quad (5)$$

*Proof.* The proof uses the positivity of the variance and minimizes  $\sigma_{\mathcal{B}}^2$  using Lagrange multipliers finding all  $\sqrt{\text{Var}_{|\psi\rangle}(H_b)}/M_b$  to be the same. See Appendix A, for details.  $\square$

As a direct consequence, Lemma 1 shows that partitioning  $H$  always increases the sampling error independently of the state  $|\psi\rangle$  and partitioning  $\mathcal{B}$  (see also Appendix A):

$$\frac{1}{M} \text{Var}_{|\psi\rangle}(H) \leq \sum_{H_b \in \mathcal{B}} \frac{\text{Var}_{|\psi\rangle}(H_b)}{M_b} \quad (6)$$

Further, Eq. (5) motivates to define the following cost function to compare measurement strategies, being different splittings of  $H$ , that is not only independent of the specific measurement budget allocation  $M_b$  but also independent of the specific number of measurements  $M$ :

**Definition 1** (Relative Sampling complexity). Let  $\mathcal{B}_1$  and  $\mathcal{B}_2$  be partitionings of  $H$ , then we call the ratio of the number of samples  $M_{\mathcal{B}_1}/M_{\mathcal{B}_2}$  to obtain the same standard error  $\sigma_{\mathcal{B}_1}^2 = \sigma_{\mathcal{B}_2}^2$  (see Eq. (5)), the relative sampling complexity:

$$\mathcal{G}_{|\psi\rangle}(\mathcal{B}_1, \mathcal{B}_2) = \frac{M_{\mathcal{B}_1}}{M_{\mathcal{B}_2}} = \left[ \frac{\sum_{H_b \in \mathcal{B}_1} \sqrt{\text{Var}_{|\psi\rangle}(H_b)}}{\sum_{H'_b \in \mathcal{B}_2} \sqrt{\text{Var}_{|\psi\rangle}(H'_b)}} \right]^2 \quad (7)$$

For  $\mathcal{G}_{|\psi\rangle}(\mathcal{B}_1, \mathcal{B}_2) > 1$ , we thus get a sampling improvement of partitioning  $\mathcal{B}_2$  compared to partitioning  $\mathcal{B}_1$ , and the value of  $\mathcal{G}_{|\psi\rangle}(\mathcal{B}_1, \mathcal{B}_2)$  tells us how much less often we have to measure within partitioning  $\mathcal{B}_2$  compared to  $\mathcal{B}_1$  for the same standard error Eq. (3) under optimal sampling budget allocation.

## B. Sampling improvement lower bounds

Many quantum algorithms aim to prepare eigenstates of Hamiltonians, including ground states. In this section, we thus consider the task of estimating energies

$E_i$  of eigenstates  $H|E_i\rangle = E_i|E_i\rangle$ . Our aim is to make statements about the sampling improvement factor  $\mathcal{G}_{|E_i\rangle}(\mathcal{B}_{\text{Pauli}}, \mathcal{B}_{L_x, L_y})$ , where  $\mathcal{B}_{\text{Pauli}}$  labels the partitioning of  $H$  into groups of mutually commuting local operators, which often coincide for lattice Hamiltonians to partitioning into different Pauli operators.  $\mathcal{B}_{L_x, L_y}$  denotes the splitting  $H$  into  $L_x \times L_y$  large disjoint patches, a cover of which forms one of the partitions of  $H$ . We call these geometric partitionings. They are defined explicitly as follows:

**Definition 2** (Explicit geometric partitionings). Let  $H$  be a lattice Hamiltonian as defined in Eq. (4). We define its geometric partitioning  $H_1 + H_2 = H$  by:

$$H_1 := \frac{1}{2} (H - H_{\text{cut}} + H'_{\text{cut}}) \quad (8)$$

$$H_2 := \frac{1}{2} (H + H_{\text{cut}} - H'_{\text{cut}}) \quad (9)$$

with  $H_{\text{cut}}$  being the 2-local terms of  $H$  cut in  $H_1$  and added to  $H_2$ , and vice versa  $H'_{\text{cut}}$  to obtain subsystem patches  $H_{b,k}$  with disjoint support. We use the notation

$$\mathcal{H}_i = \sum_{\alpha} h_i^{(\alpha)} o_i^{(\alpha)} \quad \text{and} \quad \mathcal{H}_{i,j} = \sum_{\alpha, \beta} J_{i,j}^{(\alpha, \beta)} o_i^{(\alpha)} o_j^{(\beta)} \quad (10)$$

for the one-local and two-local terms in Eq. (4), where the site indices  $i$  and  $j$  have two components for two dimensional lattices,  $i = (i_x, i_y)$  and  $j = (j_x, j_y)$ , and consider the following three specific partitionings.

a. *1D partitioning* with 1D strip width  $L$ :

$$H_{\text{cut}} = \sum_{m=1}^{\lfloor n_x/L \rfloor} \sum_{\ell=1}^{n_y} \mathcal{H}_{(mL, \ell), (mL+1, \ell)} \quad (11)$$

$$H'_{\text{cut}} = \sum_{m=1}^{\lfloor n_x/L \rfloor} \sum_{\ell=1}^{n_y} \mathcal{H}_{(mL-1, \ell), (mL, \ell)} \quad (12)$$

where  $L = 1$  is a special case with  $H_{\text{cut}}$  consisting of all 2-local terms in  $x$ -direction and respectively  $H'_{\text{cut}}$  containing all 2-local terms in  $y$ -direction.

b. *2D partitioning* with patch size  $L_x \times L_y$ :

$$\begin{aligned} H_{\text{cut}} &= \sum_{m=1}^{\lfloor n_x/L_x \rfloor} \sum_{\ell=1}^{n_y} \mathcal{H}_{(mL_x, \ell), (mL_x+1, \ell)} \\ &+ \sum_{m=1}^{n_x} \sum_{\ell=1}^{\lfloor n_y/L_y \rfloor} \mathcal{H}_{(m, \ell L_y), (m, \ell L_y+1)} \end{aligned} \quad (13)$$

$$\begin{aligned} H'_{\text{cut}} &= \sum_{m=1}^{\lfloor n_x/L_x \rfloor} \sum_{\ell=1}^{n_y} \mathcal{H}_{(mL_x-1, \ell), (mL_x, \ell)} \\ &+ \sum_{m=1}^{n_x} \sum_{\ell=1}^{\lfloor n_y/L_y \rfloor} \mathcal{H}_{(m, \ell L_y-1), (m, \ell L_y)} \end{aligned} \quad (14)$$



*c. 2-local partitioning* Further, we can partition  $H$  into  $H_b$ 's with disjoint blocks of size 2, which requires four parts  $H = H_1 + H_2 + H_3 + H_4$ :

$$H_1 = \sum_{m=1}^{\lfloor n_x/2 \rfloor} \sum_{\ell=1}^{n_y} \mathcal{H}_{(2m,\ell),(2m+1,\ell)} + \frac{1}{4} \sum_i \mathcal{H}_i \quad (15)$$

$$H_2 = \sum_{m=1}^{\lfloor n_x/2 \rfloor} \sum_{\ell=1}^{n_y} \mathcal{H}_{(2m-1,\ell),(2m,\ell)} + \frac{1}{4} \sum_i \mathcal{H}_i \quad (16)$$

$$H_3 = \sum_{m=1}^{n_x} \sum_{\ell=1}^{\lfloor n_y/2 \rfloor} \mathcal{H}_{(m,2\ell),(m,2\ell+1)} + \frac{1}{4} \sum_i \mathcal{H}_i \quad (17)$$

$$H_4 = \sum_{m=1}^{n_x} \sum_{\ell=1}^{\lfloor n_y/2 \rfloor} \mathcal{H}_{(m,2\ell-1),(m,2\ell)} + \frac{1}{4} \sum_i \mathcal{H}_i \quad (18)$$

For all considered partitionings of  $H$ , we have the following lemma.

**Lemma 2** (Variance (In-)Equalities). For a state  $|\psi\rangle$  and Hamiltonian partitioning  $H = \sum_{H_k \in \mathcal{B}} H_k$  we have:

$$|\mathcal{B}| \sum_{H_k \in \mathcal{B}} \text{Var}_{|\psi\rangle}(H_k) \geq \left( \sum_{H_k \in \mathcal{B}} \sqrt{\text{Var}_{|\psi\rangle}(H_k)} \right)^2 \quad (19)$$

$$\geq \sum_{H_k \in \mathcal{B}} (2k-1) \text{Var}_{|\psi\rangle}(H_k), \quad (20)$$

where the variance terms are without restricting the generality taken to be ordered non-increasingly as  $\text{Var}_{|\psi\rangle}(H_1) \geq \text{Var}_{|\psi\rangle}(H_2) \geq \dots$

*Proof.* Eq. (20) is a purely algebraic observation. Let us denote  $\text{Var}_{|\psi\rangle}(H_k) := a_k \geq a_{k+1} \geq 0$  and  $|\mathcal{B}| = K$ . From  $0 \leq (a-b)^2 = (a+b)^2 - 4ab$  follows  $\sqrt{ab} \leq \frac{1}{2}(a+b)$  and hence:

$$\left( \sum_{k=1}^K \sqrt{a_k} \right)^2 \leq \sum_{k=1}^K a_k + \sum_{k>\ell=1}^K (a_k + a_\ell) = K \sum_{k=1}^K a_k \quad (21)$$

Similarly, from  $\sqrt{ab} \geq \min(a,b)$  follows

$$\left( \sum_{k=1}^K \sqrt{a_k} \right)^2 \geq \sum_{k=1}^K a_k + \sum_{k=2}^K 2(k-1)a_k = \sum_{k=1}^K (2k-1)a_k \quad (22)$$

□

As an intermediate consequence for any partitioning scheme in 2 parts, and energy estimation of an eigenstate, we know that we optimally have to measure both parts equally often as both variances are the same. For instance, this applies to 1D and 2D geometric partitioning (Def. 2):

**Corollary 1** (Variance equality for eigenstate two partitionings). If  $H$  is partitioned into two parts  $H_1$  and  $H_2$  and  $|\psi\rangle = |E_i\rangle$  is an eigenstate of  $H$ , then Eq. (20) becomes an equality:

$$\text{Var}_{|E_i\rangle}(H_1) = \text{Var}_{|E_i\rangle}(H_2). \quad (23)$$

and the commutator-based lower bound (commonly named uncertainty principle [20]) vanishes:

$$|\langle E_i | [H_1, H_2] | E_i \rangle| = 0 \quad (24)$$

*Proof.* For bipartitions of eigenstates we obtain from  $\text{Var}_{|E_i\rangle}(H) = 0$ :

$$\begin{aligned} \text{Var}_{|E_i\rangle}(H_1) + \text{Var}_{|E_i\rangle}(H_2) &= 2|\text{CoV}_{|E_i\rangle}(H_1, H_2)| \\ &\leq 2\sqrt{\text{Var}_{|E_i\rangle}(H_1) \text{Var}_{|E_i\rangle}(H_2)} \end{aligned} \quad (25)$$

where we used that the covariance is an inner product and applied the Cauchy-Schwarz inequality. From  $\sqrt{ab} \leq \frac{1}{2}(a+b)$  we obtain that Eq. (25) needs to be an equality, and hence Eq. (23). Further this also implies  $\text{CoV}_{|E_i\rangle}(H_1, H_2) = \text{CoV}_{|E_i\rangle}(H_2, H_1)$ , and thus  $\langle E_i | H_1 H_2 | E_i \rangle = \langle E_i | H_2 H_1 | E_i \rangle$ . □

Furthermore, even if a Pauli partitioning  $\mathcal{B}_{\text{Pauli}}$  requires more than two non-commuting Pauli groupings, we can still restrict our considerations to the case  $H = H_1 + H_2$ . To see this, let us assume we need to partition the mutually commuting grouping measurements into 3 parts. As Eq. (6) is independent of the state, we know that measuring finer partitioned always increases the combined variance (e.g. plug in on the LHS  $H_2$  instead of  $H$ ). Hence, for finding the lower bound, it suffices to consider a two partition, where we can measure  $H_1$  and put all other terms into  $H_2$ .

To prove a sampling improvement for measuring in the eigenbases of decoupled subsystems, we express the decoupled Hamiltonians as an orbit of a subgroup of the translations along the  $x$ - and  $y$ -direction of a 2-dimensional lattice. The operators  $T_\ell^x$  and  $T_\ell^y$  denote a translation by  $\ell$  sites into the respective direction. Both direction are connected via a local rotation operation  $S$  that maps  $T_\ell^y = S T_\ell^x S$ . Altogether, we consider subgroups of the symmetry group

$$\mathcal{T} = \{T_\ell^x T_m^y | \ell = 1, \dots, n_x, m = 1, \dots, n_y\}. \quad (26)$$

With this, every  $k$ -local, translation invariant Hamiltonian can be written as an orbit of  $\mathcal{T}$  acting on a unit cell interaction  $V$ , i.e.

$$H = \sum_{T \in \mathcal{T}} T V T^\dagger + H_{1\text{-local}}. \quad (27)$$

As a matter of convention, we separate the interaction terms given by  $V = \sum_{i,j} \mathcal{H}_{i,j}$  from the 1-local field terms  $H_{1\text{-local}} = \sum_i \mathcal{H}_i$ . With this, we can quantify the reduction of shot noise of the measurement strategies depicted in Fig. 1, and more explicitly in Fig. 3. We prove the following lower bounds on the sampling improvement.

**Theorem 1** (Sampling improvement lower bound). *Let  $H$  be a translation-invariant 2-local Hamiltonian on an  $n_x \times n_y$  rectangular lattice as specified by Eq. (27). Then, for any non-degenerate eigenstate  $|E_i\rangle$  of  $H$ ,*

$$\mathcal{G}_{|E_i\rangle}(\mathcal{B}_{\text{Pauli}}, \mathcal{B}_{L_x, L_y}) \geq \begin{cases} 4L \frac{1}{1 - \text{CoR}(H_{\text{cut}}, H'_{\text{cut}})} & \text{(a)} \\ 4 \frac{L_x L_y}{L_x + L_y} \frac{1}{1 - \text{CoR}(H_{\text{cut}}, H'_{\text{cut}})} & \text{(b)} \\ \frac{4}{3} & \text{(c)} \end{cases} \quad (28)$$

where  $L$  is the length of the geometric partition for 1D cuts (a),  $L_x$  and  $L_y$  the patch size for 2D cuts (b), and (c) corresponds to the equal splitting of  $H$  into four 2-local partitions.  $\text{CoR}(A, B) = \text{CoV}(A, B) / \sqrt{\text{Var}(A) \text{Var}(B)}$  denotes the correlation.  $H_{\text{cut}}$  gives which 2-local terms of  $H$  are cut in  $H_1$  and added to  $H_2$ , and vice versa  $H'_{\text{cut}}: 2H_1 = H - H_{\text{cut}} + H'_{\text{cut}}$ . See also Def. 2

*Proof (Sketch).* In all three cases, the proof is a composition of the variance of the Hamiltonians in  $\mathcal{B}_{\text{Pauli}}$  and  $\mathcal{B}_{L_x, L_y}$  into the ones of the unit cell interaction  $V$ . The multi-linearity of the covariance and the invariance of the ground state enables an identification of terms yielding the respective factor for each case. See Appendix B for technical details.  $\square$

We have formulated Theorem 1 as a sample improvement when measuring the Hamiltonian on non-degenerate eigenstates. Note that, case (a) is not a special case of (b), as the latter cuts in both directions s.t. for example setting  $L_x = n_x$  will yield a weaker bound. It readily generalizes to other measurement schemes  $\mathcal{B}$ . A generalization from 2-local to  $k$ -local interactions is straightforward, albeit it comes with a weakening factor on the sample improvement, or respectively a scaling factor of necessary cluster lengths.

The lower bounds (a) and (b) in Theorem 1 become arbitrarily large for  $\text{CoR}(H_{\text{cut}}, H'_{\text{cut}}) \rightarrow 1$ , or equivalently  $\text{Var}_{|E_i\rangle}(H_{L_x, L_y}^{(1)}) = \text{Var}_{|E_i\rangle}(H_{L_x, L_y}^{(2)}) \rightarrow 0$ . This behavior is expected for our strategy of comparing the required measurements to achieve the same precision. One would need a diverging number of measurements to achieve the same standard error  $\sigma_{\mathcal{B}_{L_x, L_y}} \rightarrow 0$  for "naive" partitioning with  $(\sum_{H_b \in \mathcal{B}_{\text{Pauli}}} \sqrt{\text{Var}_{|E_i\rangle}(H_b)})^2 \neq 0$ .

### C. Improvement estimate for imperfect eigenstates

In real world sampling situations, where we aim for preparing eigenstates, we can typically not avoid at best small perturbations. These can originate from approximation errors of our state preparation procedure or, even for exact state preparation algorithms like [19], from imperfect operations on the quantum hardware.

Thus, in a realistic setting, we do not only have a single perfectly reproducible quantum state. Instead, we generate on our quantum computer an ensemble of states  $\{|\tilde{\psi}\rangle\}$  that are all potentially (slightly) different. As a

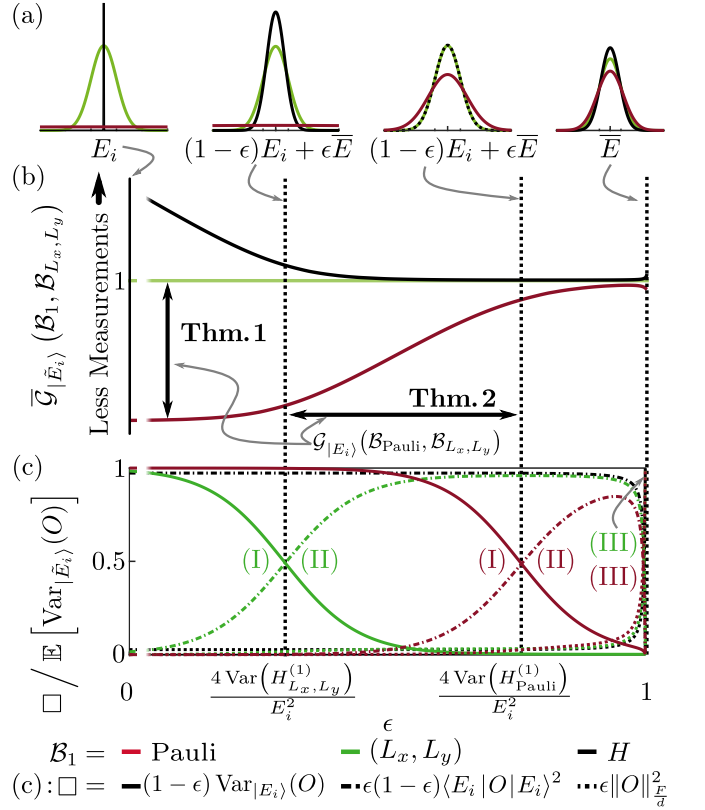


**FIG. 2. Sampling improvement: from perfect eigenstates to Haar-random states:** Here, we consider states of the form  $|\bar{E}_i\rangle = \sqrt{1-\epsilon}|E_i\rangle + \sqrt{\epsilon}|\xi\rangle$  with  $|\xi\rangle$  Haar random up to second moments. All three subplots share the same x-axis ( $\epsilon$ ) as well as color coding: red for Pauli, green for geometric, and black for eigenbasis partitioning. Following the three terms in Lemma 3, there are three regimes (see also Corollary 3). (I) Up to a noise level  $\epsilon \leq 4 \text{Var}_{|E_i\rangle}(O)/E_i^2$  the sampling improvement is effectively maintained (see Theorem 1), which is followed by an intermediate noise regime (II), where the energy square term in Eq. (31) is dominant. Eventually, in a third random-dominant regime, where  $\epsilon \geq 1 - \mathcal{O}(1/n)$ , the sampling improvements become independent of the state but are only given by the Frobenius-norms of the partitions. In (a), we show the probability density corresponding to the empirical mean estimator  $\bar{O}_M$  for different measurement strategies. The different snapshots depict  $\epsilon = 0$ ,  $\epsilon \approx 4 \text{Var}(H_{L_x, L_y}^{(1)})/E_i^2$ ,  $\epsilon \approx 4 \text{Var}(H_{\text{Pauli}}^{(1)})/E_i^2$  and  $\epsilon \approx 1$ . In (b), we provide a qualitative graph of the relative sampling complexity (Def. 3). First, measuring in the eigenbasis is perfect, then measuring in the geometric partitioning becomes comparable (up to factor 2) to sampling in the eigenbasis since it distributes the energy equally (also compare (a)). We show in Theorem. 2 that this (I)  $\rightarrow$  (II) transition happens for Pauli partitioning for  $\times \mathcal{G}_{|E_i\rangle}(\mathcal{B}_{\text{Pauli}}, \mathcal{B}_{L_x, L_y})$  larger  $\epsilon$  ("worse" prepared eigenstates). In (c) we give the relative weight of the terms (I), (II) and (III) in Eq. (31), which mark the transition from low to intermediate to fully random regime. The specific data shown here is taken for a 2D Transverse field Ising model, but the graphs will qualitatively always look alike, guaranteed by our Theorems.

consequence, we have to consider the statistical error average  $\mathbb{E}$  over this ensemble of states. Nevertheless, a

similar upper bound to Eq. (6) holds true:

$$\begin{aligned} \frac{1}{M} \mathbb{E} \left[ \text{Var}_{|\tilde{\psi}\rangle} (H) \right] &\leq \frac{1}{M} \mathbb{E} \left[ \left( \sum_{H_b \in \mathcal{B}} \sqrt{\text{Var}_{|\tilde{\psi}\rangle} (H_b)} \right)^2 \right] \\ &\leq \frac{1}{M} \left[ \sum_{H_b \in \mathcal{B}} \sqrt{\mathbb{E} \left[ \text{Var}_{|\tilde{\psi}\rangle} (H_b) \right]} \right]^2 \end{aligned} \quad (29)$$

here, we applied a second time the Cauchy-Schwarz inequality onto the expectation value over  $\{|\psi\rangle\}$ , to obtain the second inequality, which would be an equality if the different random variables  $\sqrt{\text{Var}_{|\tilde{\psi}\rangle} (H_b)}$  were stochastically independent. For the explicit calculation see Appendix A. The above inequality allows us to expand the previously defined relative sampling complexity (Definition 1) to ensembles of states:

**Definition 3** (Relative Sampling complexity of a state ensemble). Let  $\mathcal{B}_1$  and  $\mathcal{B}_2$  be partitionings of  $H$ , let  $\{|\tilde{\psi}\rangle\}$  denote a set of states and  $\mathbb{E}$  the average over these states. Then we define:

$$\bar{\mathcal{G}}_{|\tilde{\psi}\rangle} (\mathcal{B}_1, \mathcal{B}_2) := \frac{\left[ \sum_{H_b \in \mathcal{B}_1} \sqrt{\mathbb{E} \left[ \text{Var}_{|\tilde{\psi}\rangle} (H_b) \right]} \right]^2}{\left[ \sum_{H'_b \in \mathcal{B}_2} \sqrt{\mathbb{E} \left[ \text{Var}_{|\tilde{\psi}\rangle} (H'_b) \right]} \right]^2} \quad (30)$$

In typical scenarios, we aim to prepare a certain quantum state  $|\psi\rangle$ , but in reality prepared multiple slightly different states  $\{|\tilde{\psi}\rangle\} := \sqrt{1-\epsilon}|\psi\rangle + \sqrt{\epsilon}|\xi\rangle$ , with  $\{|\xi\rangle\}$  being an ensemble of quantum states. In our particular setting, we have  $|\psi\rangle = |E_i\rangle$  ( $H|E_i\rangle = E_i|E_i\rangle$ ) for a lattice Hamiltonian  $H$ . However, this is not needed within the following Lemma, which allows us to resolve  $\mathbb{E} \left[ \text{Var}_{|\tilde{\psi}\rangle} (H_b) \right]$ :

**Lemma 3** (Variance of isotropically perturbed states). Let  $|\psi\rangle \in \mathbb{C}^d$  be some fixed reference state vector,  $|\xi\rangle$  be a random vector distributed according to a spherical 2-design in  $\mathbb{C}^d$ ,  $O$  an observable, and  $\epsilon \in [0, 1]$ . Then, for  $|\tilde{\psi}\rangle := \sqrt{1-\epsilon}|\psi\rangle + \sqrt{\epsilon}|\xi\rangle$ ,

$$\begin{aligned} \mathbb{E} \left[ \text{Var}_{|\tilde{\psi}\rangle} (O) \right] &= (1-\epsilon) \text{Var}_{|\psi\rangle} (O) & (I) \\ &+ \epsilon(1-\epsilon) \langle \psi | O | \psi \rangle^2 & (II) \\ &+ \epsilon \|O\|_{\frac{F}{d}}^2 + \mathcal{O}(1/d) & (III) \end{aligned} \quad (31)$$

where  $\|\cdot\|_{\frac{F}{d}}$  denotes the Frobenius norm renormalized by a dimension factor  $d = 2^n$  for system size  $n$ .

*Proof (Sketch).* We use known results from representation theory, more concretely the Schur-Weyl duality, and the so-called swap-trick to resolve the integrals. For the explicit calculation see Appendix C.  $\square$

Within the Lemma we used that the  $\{|\xi\rangle\}$  are distributed up to the second moment indistinguishably from a Haar-random state. This is agnostic to a specific preparation algorithm and reflects that the target state can only be prepared up to an error  $\epsilon$ .

Unlike for perfect eigenstates, we have for  $\epsilon \neq 0$ ,  $\mathbb{E} \left[ \text{Var}_{|\tilde{E}_i\rangle} (H) \right] = \epsilon(1-\epsilon)E_i^2 + \epsilon \|H\|_{\frac{F}{d}}^2 + \mathcal{O}(2^{-n}) \neq 0$ . Thus,  $\mathcal{B}_1 = \mathcal{B}_H$  provides a nontrivial finite upper bound for the sampling improvement (see also Fig. 2 (c)). This means in the case of  $\epsilon \neq 0$  there will be both an upper and lower bound. To obtain these bounds, we plug Eq. (31) into Eq. (30), for the following Corollary:

**Corollary 2** (Sampling improvement upper and lower bound for imperfect eigenstates). Let  $|\tilde{E}_i\rangle = \sqrt{1-\epsilon}|E_i\rangle + \sqrt{\epsilon}|\xi\rangle$ ,  $|\xi\rangle$  be a random vector distributed according to a spherical 2-design in  $\mathbb{C}^d$ , and  $\epsilon \in [0, 1]$ . Further, let  $\mathcal{B}_{\text{Pauli}}$  be a valid Pauli partitioning and  $\mathcal{B}_{L_x, L_y}$  be a valid geometric partitioning of  $H$ . Then we have the following bounds:

$$\bar{\mathcal{G}}_{|\tilde{E}_i\rangle} (\mathcal{B}_{\text{Pauli}}, \mathcal{B}_{L_x, L_y}) \begin{cases} \leq |\mathcal{B}_{\text{Pauli}}| + \frac{|\mathcal{B}_{\text{Pauli}}|^2 \text{Var}_{|E_i\rangle} (H_{\text{Pauli}}^{(1)})}{\epsilon E_i^2 + \epsilon / (1-\epsilon) \|H\|_{\frac{F}{d}}^2} \\ \geq \frac{g_{\text{Pauli}}(\epsilon)}{g_{L_x, L_y}(\epsilon)} \end{cases} \quad (32)$$

with:

$$\begin{aligned} g_{\text{part.}}(\epsilon) &= 4(1-\epsilon) \text{Var}_{|E_i\rangle} (H_{\text{part.}}^{(1)}) + \epsilon(1+\beta_{\text{part.}}) \|H\|_{\frac{F}{d}}^2 \\ &+ \epsilon(1-\epsilon)(1+\alpha_{\text{part.}}^2) E_i^2 \end{aligned} \quad (33)$$

for the partitionings  $\text{part.} = \text{Pauli}$  and  $\text{part.} = L_x, L_y$ .  $\alpha$  quantifies the average asymmetry of the energy distribution and  $\beta$  gives the average asymmetry of squared Pauli weights across the partitions:

$$\alpha_{\text{part.}} := \left| \langle H_{\text{part.}}^{(1)} \rangle / E_i - 1/2 \right| \quad (34)$$

$$\beta_{\text{part.}} := \left| \|H_{\text{part.}}^{(1)}\|_{\frac{F}{d}}^2 / \|H\|_{\frac{F}{d}}^2 - 1/2 \right| \quad (35)$$

*Proof.* For the upper bound we use Eq. (19) to linearise the numerator:

$$\left( \sum_{H_b \in \mathcal{B}_{\text{Pauli}}} \sqrt{\mathbb{E} \left[ \text{Var}_{|\tilde{E}_i\rangle} (H_b) \right]} \right)^2 \quad (36)$$

$$\leq |\mathcal{B}_{\text{Pauli}}| \sum_{H_b \in \mathcal{B}_{\text{Pauli}}} \mathbb{E} \left[ \text{Var}_{|\tilde{E}_i\rangle} (H_b) \right] \quad (37)$$

$$\leq |\mathcal{B}_{\text{Pauli}}|^2 (1-\epsilon) \text{Var}_{|E_i\rangle} (H_{\text{Pauli}}^{(1)}) \quad (38)$$

$$+ |\mathcal{B}_{\text{Pauli}}| \epsilon(1-\epsilon) E_i^2 + |\mathcal{B}_{\text{Pauli}}| \epsilon \|H\|_{\frac{F}{d}}^2 + \mathcal{O}(2^{-n})$$

where we used that  $|\langle H_b \rangle| \leq |E_i|$ ,  $E_i = \sum_{H_b \in \mathcal{B}_{\text{Pauli}}} \langle H_b \rangle$  and hence:

$$\sum_{H_b \in \mathcal{B}_{\text{Pauli}}} \langle H_b \rangle^2 \leq E_i^2 \quad (39)$$

Further, the "naive" partitioning puts the local operators in  $H$  in exactly one  $H_b$ , which is why we have:

$$\sum_{H_b \in \mathcal{B}_{\text{Pauli}}} \|H_b\|_{\frac{F}{d}}^2 = \|H\|_{\frac{F}{d}}^2 \quad (40)$$

For the denominator, we simply plug in

$$\mathbb{E} \left[ \text{Var}_{|\tilde{E}_i\rangle} (H) \right] = \epsilon(1 - \epsilon)E_i^2 + \epsilon \|H\|_{\frac{F}{d}}^2 + \mathcal{O}(2^{-n}) \quad (41)$$

For the lower bound, it again suffices to focus on a Pauli partitioning into two parts, as splitting into more parts will lead to a larger lower bound due to Eq. (20). We plug Eq. (31) into Eq. (30). For geometric partitionings we still have

$$\mathbb{E} \left[ \text{Var}_{|\tilde{E}_i\rangle} \left( H_{L_x, L_y}^{(1)} \right) \right] = \mathbb{E} \left[ \text{Var}_{|\tilde{E}_i\rangle} \left( H_{L_x, L_y}^{(2)} \right) \right] \quad (42)$$

as splittings are symmetric, hence not only the variances [(I) in Eq. (31)], but also energies and Forbenius norms are equal [(II) and (III) in Eq. (31)]. For Pauli partitioning, we apply Eq. (20), and use Eq. (23) as well as Eq. (40).  $\square$

Note that  $\alpha_{L_x, L_y} = 0$  as geometric partitioning distributes the energy and Pauli weights equally. Thus, Eq. (32) generalizes Eq. (28) to imperfect eigenstates, with a random perturbation according to a spherical 2-design in  $\mathbb{C}^d$ . As before, for Pauli splittings, partitionings with  $|\mathcal{B}| = 2$  provide lower bounds to partitionings with  $|\mathcal{B}| > 2$  due to Eq. (20). Hence in the worst case, we underestimate the improvement of geometric partitioning compared to the mutually commuting operator grouping baseline. Further, Corollary 2 allows us to decide in a scalable fashion for lattice Hamiltonians and for any  $\epsilon \in [0, 1]$  whether a given geometric partitioning yields a sampling improvement:

**Lemma 4** (Criterion for noise-level independent advantage of geometric partitioning). As before, let  $|\tilde{E}_i\rangle = \sqrt{1 - \epsilon}|E_i\rangle + \sqrt{\epsilon}|\xi\rangle$ ,  $|\xi\rangle$  be a random vector distributed according to a spherical 2-design in  $\mathbb{C}^d$ , and  $\epsilon \in [0, 1]$ . Further, let  $\mathcal{B}_{\text{Pauli}}$  be a valid Pauli partitioning and  $\mathcal{B}_{L_x, L_y}$  be a valid geometric partitioning of  $H$ . Then we have

$$\bar{\mathcal{G}}_{|\tilde{E}_i\rangle}(\mathcal{B}_{\text{Pauli}}, \mathcal{B}_{L_x, L_y}) \geq 1 \quad (43)$$

iff

$$\bar{\mathcal{G}}_{|\xi\rangle}(\mathcal{B}_{\text{Pauli}}, \mathcal{B}_{L_x, L_y}) = \left( \frac{\sum_{H_b \in \mathcal{B}_{\text{Pauli}}} \|H_b\|_F}{\sum_{H'_b \in \mathcal{B}_{L_x, L_y}} \|H'_b\|_F} \right)^2 \geq 1 \quad (44)$$

which can be evaluated efficiently classically for lattice Hamiltonians.

*Proof.* We can apply following algebraic inequality iteratively to Eq. (32), where  $A, A', B, B' \geq 0$ :

$$\frac{A}{A'} \geq \frac{B}{B'} \Rightarrow \frac{A}{A'} \geq \frac{A+B}{A'+B'} \geq \frac{B}{B'} \quad (45)$$

To see that Eq. (45) holds add  $AA'$  or  $BB'$  to  $AB' \geq BA'$  and resolve for  $A/A'$  or  $B/B'$ . This lets us lower bound the sampling improvement by:

$$\bar{\mathcal{G}}_{|\tilde{E}_i\rangle}(\mathcal{B}_{\text{Pauli}}, \mathcal{B}_{L_x, L_y}) \geq \min \left( \frac{A'}{A}, \frac{B'}{B}, \frac{C'}{C} \right) \quad (46)$$

with  $A, B, C$  being the summed terms in Eq. (33),  $A'/A = \mathcal{G}_{|E_i\rangle}(\mathcal{B}_{\text{Pauli}}, \mathcal{B}_{L_x, L_y})$  is given by Theorem 1,  $B'/B = (1 + \alpha_{\text{Pauli}}^2) \geq 1$  as geometric partitioning equally distributes the energy and  $C'/C$  is given by Eq. (44).  $\square$

Besides a criterion that geometric partition will always perform better than mutually commuting operator grouping, Eq. (44) can be interpreted as a state independent cost function [14]. Its value tells us – on average – what improvement we can expect by geometric partitioning compared to Pauli partitioning for an arbitrary state. Thus, even if we cannot take advantage of any state structure, we can still improve our measurement scheme on the observable partitioning level by optimizing Eq. (44). However, the following corollary tells us that in this case the best case improvement we can hope for is upper bound by  $|\mathcal{B}|$ :

**Corollary 3** (Sampling improvement regimes). Eq. (32) gives us three regimes for randomly perturbed eigenstates:

- I. *Low randomness*,  $\epsilon \leq 4 \text{Var}_{|E_i\rangle}(O) / E_i^2$ :  
The sampling improvement is at worst reduced by a factor 2 compared to the  $\epsilon = 0$  case:

$$\bar{\mathcal{G}}_{|\tilde{E}_i\rangle}(\mathcal{B}_{\text{Pauli}}, \mathcal{B}_{L_x, L_y}) \geq \frac{1}{2} \mathcal{G}_{|E_i\rangle}(\mathcal{B}_{\text{Pauli}}, \mathcal{B}_{L_x, L_y}) + \mathcal{O}\left(\frac{1}{n}\right)$$

- II. *Intermediate randomness*,  $\epsilon > 4 \text{Var}_{|E_i\rangle}(O) / E_i^2$ :  
The partitioning is at worst a factor of 2 (geometric) or 3 (Pauli) worse than measuring in the eigenbasis:

$$\bar{\mathcal{G}}_{|\tilde{E}_i\rangle}(\mathcal{B}, \mathcal{B}_H) \leq 2(+1)$$

- III. *Random dominated*;  $\epsilon \geq 1 - \|H\|_{\frac{F}{d}}^2 / E_i^2$ :  
The sampling effort becomes independent of the eigenstate component, and is up to  $\mathcal{O}(|\mathcal{B}_1| |\mathcal{B}_2|)$  the same for all partitionings:

$$|\mathcal{B}_1| + \mathcal{O}\left(\frac{1}{n}\right) \geq \bar{\mathcal{G}}_{|\tilde{E}_i\rangle}(\mathcal{B}_1, \mathcal{B}_2) \geq \frac{1}{|\mathcal{B}_2|} + \mathcal{O}\left(\frac{1}{n}\right)$$

*Proof.* Case (I):

We use that for geometrically local models in the low energy spectrum  $E_i = \mathcal{O}(n)$  and  $\|H\|_{\frac{F}{d}}^2 = \mathcal{O}(n)$  so that  $\|H\|_{\frac{F}{d}}^2 / E_i^2 = \mathcal{O}(1/n)$ . Similarly,  $\text{Var}_{|E_i\rangle}(H_1)$  is extensive ( $\mathcal{O}(n)$ ) as the observable  $H_1$  is geometrically local and



thus extensive. Hence  $\epsilon = \mathcal{O}(1/n)$  and:

$$\begin{aligned}
& \bar{\mathcal{G}}_{|\tilde{E}_i\rangle}(\mathcal{B}_{\text{Pauli}}, \mathcal{B}_{L_x, L_y}) \\
& \geq \frac{4(1-\epsilon) \text{Var}_{|E_i\rangle}(H_{\text{Pauli}}^{(1)}) + \epsilon(1-\epsilon)E_i^2 + \epsilon\|H\|_{\frac{F}{d}}^2}{4(1-\epsilon) \text{Var}_{|E_i\rangle}(H_{L_x, L_y}^{(1)}) + \epsilon(1-\epsilon)E_i^2 + 2\epsilon\|H\|_{\frac{F}{d}}^2} \\
& = \frac{4(1-\epsilon) \text{Var}_{|E_i\rangle}(H_{\text{Pauli}}^{(1)}) + \epsilon(1-\epsilon)E_i^2}{4(1-\epsilon) \text{Var}_{|E_i\rangle}(H_{L_x, L_y}^{(1)}) + \epsilon(1-\epsilon)E_i^2} + \mathcal{O}\left(\frac{1}{n}\right) \\
& \geq \frac{4(1-\epsilon) \text{Var}_{|E_i\rangle}(H_{\text{Pauli}}^{(1)}) + \epsilon(1-\epsilon)E_i^2}{8(1-\epsilon) \text{Var}_{|E_i\rangle}(H_{L_x, L_y}^{(1)})} + \mathcal{O}\left(\frac{1}{n}\right) \\
& \geq \frac{1}{2}G_{|E_i\rangle}(\mathcal{B}_{\text{Pauli}}, \mathcal{B}_{L_x, L_y}) + \mathcal{O}\left(\frac{1}{n}\right)
\end{aligned}$$

Case (II):

For both Pauli and geometric two partitioning  $H = H_1 + H_2$  we have ( $\tilde{c} = 1$  for Pauli, and 0 otherwise):

$$\begin{aligned}
& \bar{\mathcal{G}}_{|\tilde{E}_i\rangle}(\mathcal{B}, \mathcal{B}_H) \\
& \leq \frac{4(1-\epsilon) \text{Var}_{|E_i\rangle}(H_1) + \epsilon(1-\epsilon)(1+\tilde{c})E_i^2 + 2\epsilon\|H\|_{\frac{F}{d}}^2}{\epsilon E_i^2 + \epsilon\|H\|_{\frac{F}{d}}^2} \\
& = 1 + \frac{4 \text{Var}_{|E_i\rangle}(H_1) + \epsilon\tilde{c}E_i^2 + \frac{\epsilon}{1-\epsilon}\|H\|_{\frac{F}{d}}^2}{\epsilon E_i^2 + \frac{\epsilon}{1-\epsilon}\|H\|_{\frac{F}{d}}^2} \leq 2 + \tilde{c}
\end{aligned}$$

Case (III):

We have  $\mathcal{O}(1/n) = \|H\|_{\frac{F}{d}}^2/E_i^2 \geq 1-\epsilon$ . Hence, the (I)-type terms are  $\mathcal{O}(1)$ , but the (II)- and (III)-type terms are  $\mathcal{O}(n)$ :

$$\bar{\mathcal{G}}_{|\tilde{E}_i\rangle}(\mathcal{B}_1, \mathcal{B}_2) = \frac{(1-\epsilon)c_1E_i^2 + c_2\|H\|_{\frac{F}{d}}^2}{(1-\epsilon)c_3E_i^2 + c_4\|H\|_{\frac{F}{d}}^2} + \mathcal{O}\left(\frac{1}{n}\right)$$

then the statement follows from  $0 \leq (1-\epsilon) \leq \|H\|_{\frac{F}{d}}^2/E_i^2$ ,  $1 \leq c_1, c_2 \leq |\mathcal{B}_1|$ , and  $1 \leq c_3, c_4 \leq |\mathcal{B}_2|$ .  $\square$

Note here the seamless transition between regime (I) and (II). Similarly, the statement in regime (II) remains true in regime (III). First, for small random perturbation of an eigenstate, we are maximally a factor 2 worse than the lower bound in Theorem 1, and afterwards geometric partitioning is maximally a factor 2 worse than the upper bound given by the eigenbases. For an illustration of the randomness regime transitions see also Figure 2 (b). To see that indeed all three regimes are realized note that for  $\epsilon \rightarrow 0$  all but the (I)-type terms vanish and respectively for  $\epsilon \rightarrow 1$  all but the (III)-type terms vanish. The intermediate randomness regime also exists, as  $\text{Var}_{|E_i\rangle}(H_1)$  is extensive ( $\mathcal{O}(n)$ ) since the observable  $H_1$  is geometrically local, and thus extensive. Similarly, for geometrically local models  $E_i = \mathcal{O}(n)$  in the low energy spectrum, and therefore  $4 \text{Var}_{|E_i\rangle}(O)/E_i^2 = \mathcal{O}(1/n)$ ,  $\|H\|_{\frac{F}{d}}^2 = \mathcal{O}(n)$ , as well as  $\|H\|_{\frac{F}{d}}^2/E_i^2 = \mathcal{O}(1/n)$ . As a consequence, the (II)-type regime is realized for  $\epsilon = \Omega(1/n)$  and  $1-\epsilon = \Omega(1/n)$ . Compare also Figure 2 (a) and Figure 5 (a).

In particular, this means that even in the fully random case (III) the maximal sampling complexity improvement of any alternative partition compared to mutually unbiased Pauli bases is upper bounded by the number of required Pauli bases  $|\mathcal{B}_{\text{Pauli}}| = 2^k + 1$ , with locality  $k$ , e.g. for 2-local  $2^k + 1 = 5$ . Consequently, even for fully random states and specific observables there can be a sampling improvement, which may appear unexpected. Importantly, we can determine the right-hand side of Eq. (44) classically at scale by simply evaluating the Frobenius norms to explicitly determining this sampling improvement. As we know the Pauli sum representation of our sparse observables  $H_b$ , and we have for Paulistring  $P_i : \text{Tr}(P_i P_j) = \delta_{i,j}$ , calculating the Frobenius norm boils down to summing the squared Pauli sum coefficients  $\|H_b\|_F^2 = \sum_{c_j P_j \in H_b} c_j^2$ .

So far, we have studied how a fixed Haar-random perturbation of strength  $\epsilon$  influences the sampling improvement  $\bar{\mathcal{G}}_{|\tilde{E}_i\rangle}(\mathcal{B}_{\text{Pauli}}, \mathcal{B}_{L_x, L_y})$  of geometric sampling, where we saw that it drops from  $\mathcal{G}_{|E_i\rangle}(\mathcal{B}_{\text{Pauli}}, \mathcal{B}_{L_x, L_y})$  for  $\epsilon = 0$  to  $\leq |\mathcal{B}_{\text{Pauli}}|$  for  $\epsilon = 1$ . This corresponds to the distance in  $y$ -direction in Fig. 2 (c). This gives rise to the orthogonal question, given a tolerable sampling overhead  $\delta$  compared to measuring in the eigenbasis of  $H$ . How much better (smaller  $\epsilon$ ) can our approximated eigenstate  $|\tilde{E}_i\rangle$  be before the sampling effort becomes  $\geq \delta$ ? This is equivalent to estimating the distance in  $x$ -direction in Fig. 2 (c). We have the following theorem:

**Theorem 2** ( $\epsilon$ -threshold for  $\delta$  sampling overhead compared to measuring in the eigenbasis). *Let  $|\tilde{E}_i\rangle = \sqrt{1-\epsilon}|E_i\rangle + \sqrt{\epsilon}|\xi\rangle$ ,  $|\xi\rangle$  be a random vector distributed according to a spherical 2-design in  $\mathbb{C}^d$ , and  $\epsilon \in [0, 1]$ . Further, let  $\mathcal{B}_{\text{Pauli}}$  be a valid Pauli partitioning and  $\mathcal{B}_{L_x, L_y}$  be a valid geometric partitioning of  $H$ , and  $\delta \geq |\mathcal{B}|$  the sampling overhead compared to the eigenbasis  $\mathcal{B}_H$ . Then there exists  $\epsilon^{(\text{threshold})} > 0$  for both Pauli and geometric partitioning s.t.:*

$$\forall \epsilon \geq \epsilon_{\text{Pauli}/L_x, L_y}^{(\text{threshold})} : \bar{\mathcal{G}}_{|\tilde{E}_i\rangle}(\mathcal{B}_{\text{Pauli}/L_x, L_y}, \mathcal{B}_H) \leq \delta + 1 \quad (47)$$

and the ratio of those noise thresholds is given by:

$$\frac{\epsilon_{\text{Pauli}}^{(\text{threshold})}}{\epsilon_{L_x, L_y}^{(\text{threshold})}} = \mathcal{G}_{|E_i\rangle}(\mathcal{B}_{\text{Pauli}}, \mathcal{B}_{L_x, L_y}) \left( \frac{\delta}{\delta - \alpha^2} \right) + \mathcal{O}\left(\frac{1}{n}\right) \quad (48)$$

where  $\alpha$  is the asymmetry of the energy distribution within the Pauli partitioning.

*Proof.* The existence of such a  $\epsilon^{(\text{threshold})}$  follows directly from Corollary 3 case (III) as well as that  $\text{Var}_{|E_i\rangle}(H) = 0$ . To show Eq. (48) we use again  $\mathcal{O}\left(\|H\|_{\frac{F}{d}}^2/E_i^2\right) = \mathcal{O}(1/n)$  to truncate the norm terms in Eq. (30). Then we do a similar calculation to Corollary 2, but with two different perturbation strengths  $\epsilon$  for Pauli and geometric

partitioning:

$$\begin{aligned} \delta + 1 &\stackrel{!}{=} \bar{\mathcal{G}}_{|\tilde{E}_i\rangle}(\mathcal{B}_{Pauli/L_x, L_y}, \mathcal{B}_H) \\ &= \frac{4 \text{Var}_{|E_i\rangle}(H_1) + \epsilon^{(\text{threshold})}(1 + \alpha^2)E_i^2}{\epsilon^{(\text{threshold})}E_i^2} + \mathcal{O}\left(\frac{1}{n}\right) \\ &= 1 + \alpha^2 + \frac{4 \text{Var}_{|E_i\rangle}(H_1)}{\epsilon^{(\text{threshold})}E_i^2} + \mathcal{O}\left(\frac{1}{n}\right) \end{aligned}$$

As  $\alpha^2 = 0$  for geometric partitioning we have:

$$\begin{aligned} \frac{\epsilon_{Pauli}^{(\text{threshold})}}{\epsilon_{L_x, L_y}^{(\text{threshold})}} &= \left( \frac{4 \text{Var}_{|E_i\rangle}(H_{Pauli}^{(1)})}{E_i^2(\delta - \alpha^2)} \right) \\ &\cdot \left( \frac{E_i^2 \delta}{4 \text{Var}_{|E_i\rangle}(H_{L_x, L_y}^{(1)})} \right) + \mathcal{O}\left(\frac{1}{n}\right) \\ &= \mathcal{G}_{|E_i\rangle}(\mathcal{B}_{Pauli}, \mathcal{B}_{L_x, L_y}) \left( \frac{\delta}{\delta - \alpha^2} \right) + \mathcal{O}\left(\frac{1}{n}\right) \end{aligned}$$

□

#### D. Numerical tests of perfect eigenstate results

Here, we provide six numerical examples illustrating our analytic results. All examples are on a two-dimensional  $(n_x, n_y) = (4, 6)$  rectangular lattice with periodic boundaries, apart from the (spinful) Fermi-Hubbard model, which also uses 24 qubits on a  $3 \times 4$  lattice. Namely, these are the 2D Transverse Field XY-Model (Sec. IID 1), the 2D Transverse Field Ising-Model (Sec. IID 2), and the 2D Transverse Field Biaxial Next-Nearest Neighbor Ising Model (Sec. IID 3) which are illustrated in Fig. 3. The second half of the examples being the Hard-Core Bose Hubbard Model (Sec. IID 4), the spinless (Sec. IID 5) and the spinful Fermi-Hubbard model (Sec. IID 6) are shown in Fig. 4.

##### 1. Two-dimensional Transverse Field XY-Model

Theorem 1 indicates that measuring via geometric partitionings can become (almost) as good as via the eigenbasis. The relative sampling complexity improvement lower bound comparing geometric partitioning with mutually commuting local operator grouping, which mostly coincides with Pauli partitioning for simple lattice models, can even diverge for  $CoR(H_{cut}, H'_{cut}) \rightarrow 1$ . This means that a specific eigenstate correlates parts of the Hamiltonian  $H_{cut}$  and  $H'_{cut}$  very efficiently. Plausible candidates are highly entangled states, for instance around zero-temperature (= ground state) phase transitions, where typically band gaps close. If  $H_{cut}$  and  $H'_{cut}$  have at least one lattice site in common, then their graph distance is 0. This applies, for example, for  $L = 1$  or  $(L_x, L_y) = (2, 2)$ . Then e.g. the Hastings-Koma lemma [21] does not yield an upper bound on the covariance making these specific

geometric partitionings particularly well-suited candidates for divergent relative sampling complexity improvements.

Indeed, with the 2D Transverse Field XY-Model [22], we were able to identify such an example, which is described by the following Hamiltonian:

$$\begin{aligned} H_{\text{TFXYM}} &= -\frac{1}{2} \sum_{\langle i, j \rangle} ((1 + \eta)X_i X_j + (1 - \eta)Y_i Y_j) \\ &\quad - h \sum_i Z_i \end{aligned} \quad (49)$$

with anisotropy parameter  $\eta$ . Note that for  $\eta = 1$ , we would obtain a Transverse Field Ising model with  $J = h = 1$ , which we show as a second example (see Section IID 2).  $H_{\text{TFXYM}}$  has three phases, a paramagnetic, a ferromagnetic and an oscillatory one. This 'oscillatory' phase is a type of ferromagnetic phase with oscillating band gap [23]. The phase boundary between ferromagnetic and oscillatory phase is at  $\eta^2 + (h/2)^2 = 1$  [22].

Hence, we fix  $\eta$  or  $h$  to scan the other parameter over the phase transition. In Fig. 3 (a) we set  $h = 1$  and scan  $\eta$ . Indeed, we find around the phase transition,  $\eta \approx \sqrt{3}/2$ , as predicted by Theorem 1 for  $L = 1$  (light green),  $L = 2$  (cyan) as well as  $(L_x, L_y) = (2, 2)$  (dashed light green, nearly not distinguishable from  $L = 1$ ) a divergence of the relative sampling improvement compared to Pauli partitioning. In addition, this divergence is also realized for the geometric 2-local partitioning (dashed yellow) providing an example that also the easier-to-implement (c)-type measurement strategies in Theorem 1 can exhibit diverging relative sampling complexity improvements, even though we were not able to show this analytically. Further, the TFXYM is an example for the extension of Theorem 1, which is proven for Pauli-2-partitions, onto  $\geq 2$ -Pauli-partitions due to Eq. (6).

##### 2. Two-dimensional Transverse field Ising-Model

Another way to search for large sampling improvement examples is to take the relative sampling complexity definition (Def. 1) directly and to look out for cases where  $\text{Var}_{|E_i\rangle}(H_1) = \text{Var}_{|E_i\rangle}(H_2)$  scale more beneficial than Pauli partitioning. One such instance is one standard test bed of quantum spin models, the 2D Transverse Field Ising Model [24–26]:

$$\mathcal{H}_{\text{TFIM}} = -J \sum_{\langle i, j \rangle} Z_i Z_j - h \sum_i X_i \quad (50)$$

which has a phase transition at  $h_c \approx 3.044J$  [27], where it exhibits a ferromagnetic phase for  $h < h_c$  and a paramagnetic phase for  $h > h_c$ . We show the following Lemma:

**Lemma 5** (Perturbative improvement estimations). The sampling complexity improvement of estimating the ground state energy  $E_0$  of the 2D TFIM on a rectangular lattice of geometric partitioning compared to Pauli

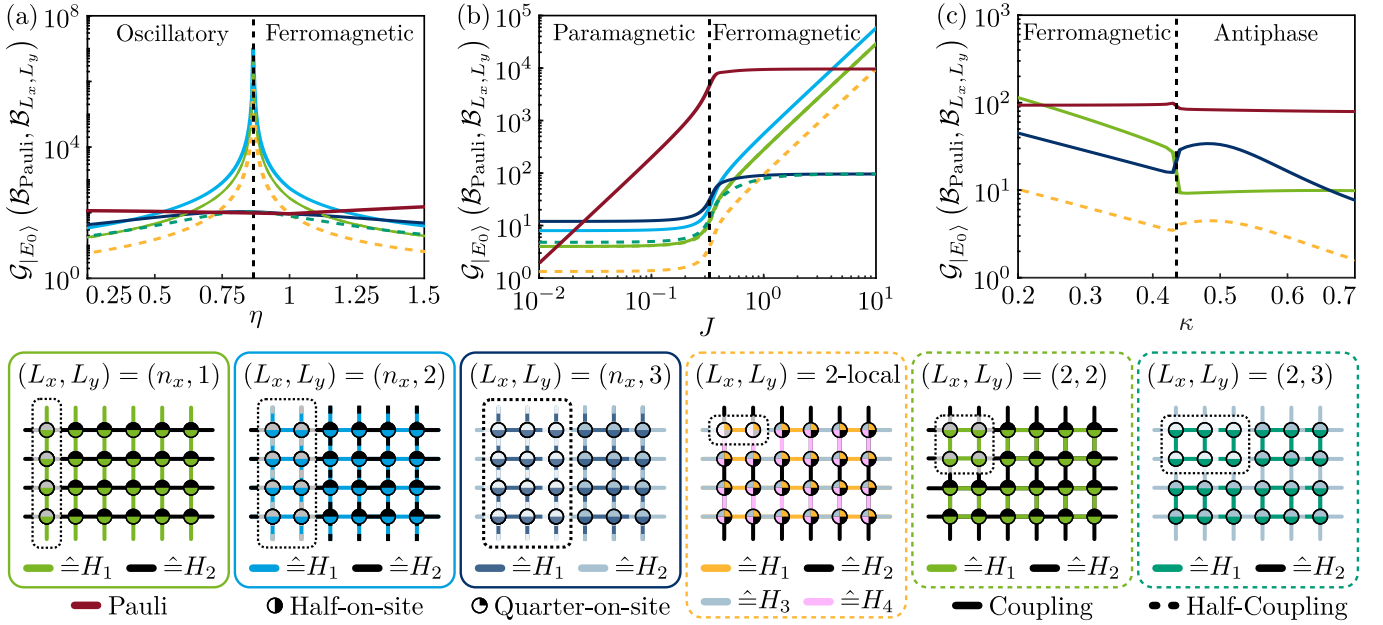


FIG. 3. **Numerical examples: TFXYM, TFIM and TF-BNNNI.** These are examples for the application of Theorem 1. All Examples are on a  $4 \times 6$  rectangular lattice with periodic boundary conditions. Critical points of phase transitions are indicated with dotted lines and the different geometric splittings are color-coded (compare legend). In the legend, the dotted boxes show the size of the unit cell, for which one needs to find a  $U_m$  in a geometric partitioning, compare also Fig. 1. In red, the absolute value of the sampling cost for Pauli measurements is given (Dividing it by the number of measurements  $M$  will give the measurement error upper bound in Eq. (6)). (a) 2D Transverse field XY-model (TFXYM): For  $\eta \rightarrow \eta_c$  (here:  $\eta_c = \sqrt{3}/2$ ) the improvement increases and diverges around the phase transition, where correlation lengths increase (Compare Eq. (28) (a)). (b) 2D Transverse Field Ising Model (TFIM). For  $J/h \ll 1$  this is an example where lower bounds are approximately realized. In contrast, for  $J/h \gg 1$ , we see improvements noticeably surpassing the lower bounds, with scalings of  $16L$  up to  $\mathcal{O}((J/h)^2)$ . For details see Lemma 5. Here the Pauli cost is multiplied by 100 to fit the common scale. (c) 2D Transverse Field Biaxial Next Nearest Neighbor Ising (BNNNI) Model.  $\kappa$  is the NNN coupling, where  $\kappa = 0$  corresponds to the TFIM. As the interaction range for this model is that of a 3-local Hamiltonian, less geometric partitionings are available for the considered lattice sizes.

sampling is given by:

$$\mathcal{G}_{|E_0\rangle}(\mathcal{B}_{\text{Pauli}}, \mathcal{B}_{L_x, L_y}) = \begin{cases} 4L + \mathcal{O}(\lambda) & \lambda = J/h \ll 1 \\ \mathcal{O}(\frac{1}{\lambda^2}) & \lambda = h/J \ll 1, L \leq 2 \\ 32L + \mathcal{O}(\lambda^2) & \lambda = h/J \ll 1, L > 2 \\ 16L + \mathcal{O}(\lambda^2) & \lambda = h/J \ll 1, i_c > 1 \end{cases} \quad (51)$$

*Proof (Sketch).* The Lemma follows from tedious, but straight forward second perturbation theory calculations of the respective variances. See Appendix D.  $\square$

This means that for  $J/h \ll 1$  the lower bounds (a) in Theorem 1 are saturated, and hence tight. In all three cases: 1D cuts (a), 2D cuts (b) and 2-local partitions (c) do the numerical results (Fig. 3 (b)) saturated the lower bounds indicating that we cannot hope for larger lower bounds within the given setting.

Furthermore, for  $J/h \gg 1$  we find within the numerical example for  $L \leq 2$ ,  $(L_x, L_y) = (2, 2)$  as well as 2-local geometric partitioning a model parameter dependent improvement of order  $\mathcal{O}((J/h)^2)$ , which matches Lemma 5 for  $L \leq 2$ . Even though our Theorem 1 gives a stronger lower bound for larger geometric partitions, this is an

example for the possibility that smaller and thus easier to implement geometric partitions can yield a higher relative sampling complexity advantage.

### 3. Two-dimensional Transverse field biaxial next-nearest-neighbour Ising model

To arrive at a model, which we need to partition similarly to an (axial) 3-local one, we can add an axial next nearest-neighbor  $Z_i Z_j$  interaction to the TFIM. Then, we obtain on a two-dimensional rectangular lattice the Transverse field biaxial next-nearest-neighbour Ising (TF-BNNNI) model [28, 29]:

$$H_{\text{TF-BNNNI}} = J \left( - \sum_{\langle i, j \rangle} Z_i Z_j + \kappa \sum_{\langle\langle i, j \rangle\rangle} Z_i Z_j \right) - h \sum_i X_i. \quad (52)$$

The TF-BNNNI model exhibits three distinct phases, e.g. compare Ref. [29] Fig. 2. For  $J = 1$  (to fix the energy scale),  $h = 0$ , and  $\kappa < \kappa_c = \frac{1}{2}$ , the nearest

neighbor coupling dominates and the ground state is ferromagnetically ordered. If  $\kappa$  becomes larger than 0.5, it becomes energetically favorable that  $2 \times 2$  plaquettes are aligned and neighboring plaquettes are flipped with respect to each other. Thus, the BNNI model can be viewed as a basic spin model for magnetic frustration.

Still, without a transverse field, the model remains diagonal or classical, and the eigenstate sampling task trivial as all eigenstates are computational basis states. In the limit  $h \rightarrow \infty$  the ground state becomes a disordered  $X$  eigenstate. For our demonstration of how geometric partitioning works for a (quasi)-3-local model, we chose  $h = 1$ , and then  $\kappa_c \approx 0.435$  (compare Figure 3 (c)). Compared to the 2-local next-nearest-neighbor models, we will consequently need to pick larger geometric partitions. The  $L = 1$ -partitioning (light green) still works as NNN coupling is axial and both partitions are rotated with respect to each other. In contrast, the  $L = 2$ -cutting would not allow to include the NNN-terms, which is why the only other one-dimensional cut is  $L = 3$  (dark blue, leading to 3 parts). Similarly, the 4 2-local partitions become 6 axial 3-local partitions (dotted yellow), or for larger systems 4 axial 5-local. In Figure 4 (b) we do not show two-dimensional patches as the smallest one would be  $3 \times 3$  (3 partitions), which is a bad fit to our  $4 \times 6$  toy model lattice, and  $4 \times 3$  would already correspond to the one-dimensional  $L = 3$  cut. For a minimal partitioning  $H = H_1 + H_2$  for an axial 3-local model, the patches would need to be  $5 \times 5$  or  $L = 5$ , which are still sufficiently small to diagonalize classically. Then all NNN couplings of a central site can be included within one patch and the unit cell can be shifted by 2 sites to cover the, previously left out, next-nearest neighbor couplings. To test these cases in 2D, one would need to consider models at least on a  $5 \times 10$  or  $10 \times 10$  lattice.

#### 4. Two-dimensional hard-core Bose-Hubbard model

If we parameterize the TFXYM, see Eq. (49), with a symmetric interaction strength  $J$ ,

$$H_{\text{HCBH}} = -\frac{J}{2} \sum_{\langle i,j \rangle} (X_i X_j + Y_i Y_j) + \frac{h}{2} \sum_i Z_i \quad (53)$$

we obtain an Hamiltonian equivalent to the hard-core limit of the Bose Hubbard model [30, 31]

$$H_{\text{HCBH}} = -J \sum_{\langle i,j \rangle} (a_i^\dagger a_j + a_i a_j^\dagger) + h \sum_i n_i \quad (54)$$

with  $a_i$ ,  $a_i^\dagger$  and  $n_i = a_i^\dagger a_i$  being bosonic annihilation, creation and number operators at lattice side  $i$  respectively.  $\langle i, j \rangle$  indicates nearest neighbors on a rectangular lattice. Compared to Bose-Hubbard model [32], in the hard-core limit the on-site repulsion term  $U/2 \sum_i n_i (n_i - 1)$  is "frozen" out as  $U \rightarrow \infty$ . Hence, the system is described by Eq. (54) with the constraint that a lattice side can

maximally be occupied by up to one boson due to the infinite on-site repulsion. This means that each lattice site is only a two-level system, and the Hilbert space of the model is "only"  $2^n$ -dimensional. Further, the number operator  $\sum_i n_i$  (or respectively  $\sum_i Z_i$ ) commutes with the Hamiltonian, and thus gives an excitation number conservation symmetry, separating the Hilbert space into  $n + 1$   $\binom{n}{m}$ -large sectors ( $m \in \{0, \dots, n\}$ ) [33]. Hence, for  $J \gtrsim h/4$ , we are in the one-dimensional all (non-)occupied sector, where the ground state is simply a  $Z$  eigenstate.

The numerical results for this model are shown in Figure 4 (a), where for  $J \gtrsim h/4$  the ground state is a  $Z$  eigenstate. In turn, the configuration space becomes the largest, and hence the model most complex, if about half the sides are occupied ( $m = n/2$ ), which is the case for the  $4 \times 6$  hard-core Bose-Hubbard model for  $0.4h \gtrsim J \gtrsim 0.47h$ . Still, we find also in this most challenging regime sampling improvements of geometric partitioning  $\mathcal{G}_{|E_i\rangle} (\mathcal{B}_{\text{Pauli}}, \mathcal{B}_{L_x, L_y})$  ranging from ca. 5 to 40.

#### 5. Two-dimensional Spinless Hubbard Model

Next, we want to demonstrate, how our geometric sampling idea is well applicable to fermionic lattice models as well. For these models, we geometrically partition the Hamiltonian in the fermionic Fock basis and then perform a local fermion-to-qubit mapping for each patch separately (together with the transformations  $U_{b,k}$ ). We start with a model of interacting fermions, that is from a lattice perspective similar to the hard-core Bose Hubbard model, just that fermions live on the lattice sites. Thus, we name this model here spinless Hubbard model:

$$H_{\text{Spinless Hubbard}} = -t \sum_{\langle i,j \rangle} (c_i^\dagger c_j + c_j^\dagger c_i) + U \sum_{\langle i,j \rangle} n_i n_j - \mu \sum_i n_i \quad (55)$$

Here  $c_i$ ,  $c_i^\dagger$  and  $n_i = c_i^\dagger c_i$  label annihilation, creation and number operators for Fermions. The  $t$ -term implements fermionic hopping between neighboring sides on the rectangular lattice, where we set  $t = 1$  to fix the energy scale. The  $U$ -term (for  $U > 0$ ) penalizes the nearest neighbor occupation [34]. Thus, for zero on-site energy  $\mu = 0$ , the model remains below half-filling ( $\sum_i n_i < n/2$ ). Similarly to the hard-core Boson Hubbard model, the number operator  $\hat{N} = \sum_i n_i$  commutes with the Hamiltonian, is hence a symmetry, and as a consequence sub-divides the Hilbert space into  $\binom{n}{m}$ ,  $m \in \{0, \dots, n\}$  large subspaces.

From this one would conclude, that the largest sub-Hilbert space occurs for  $m = n/2$ , at half filling, but at this point the system has a further conserved quantity due to a particle-hole symmetry. Thus, we identify as a challenging scenario, systems close to half-filling, but not exactly half filled  $n/2 \approx m \neq n/2$ . For the  $4 \times 6$  lattice model, we consider here, this is realized for  $\mu = 0$  and  $U \gtrsim 0.6$ , where we have  $\langle \hat{N} \rangle = 11$  (compare Figure 4



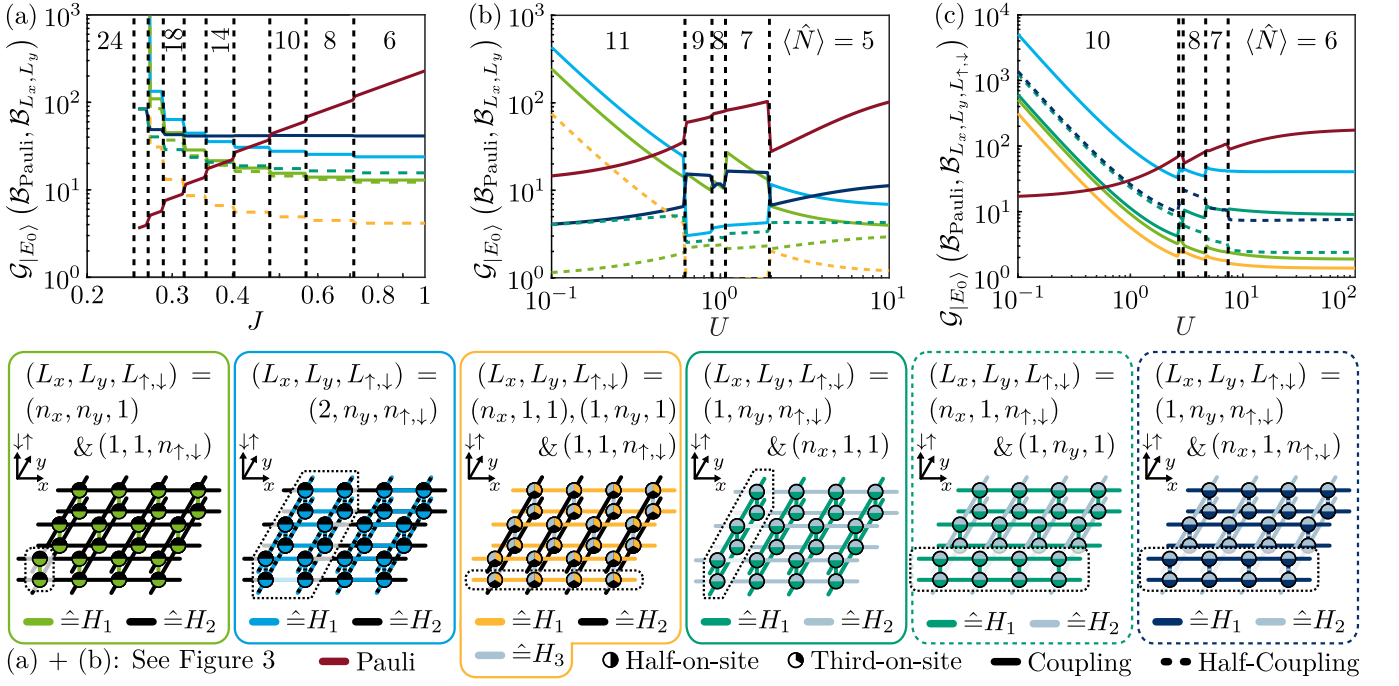


FIG. 4. **Numerical examples: Hubbard-type models.** The spinless examples (a) and (b) are on a  $4 \times 6$  rectangular lattice with periodic boundary conditions. Their partitionings and colors, including solid and dashed lines, correspond to the ones in Fig. 3. Dashed vertical lines indicate transitions between symmetry sectors of different particle number, and the different geometric splitting are color-coded. In red the absolute value of the sampling cost for Pauli measurements is shown, dividing it by the number of measurements  $M$  will give an upper bound on the standard error (compare Eq. (6)). (a) Hard-core Bose Hubbard (HCBH) model. This model is similar to the TFXYM where the XY-couplings are tuned symmetrically. The numbers show the amount of bosons in the system  $\langle E_0 | \hat{N} | E_0 \rangle$ . (b) Spinless Fermi Hubbard model. This model resembles the HCBH model, but with fermions instead of bosons on the lattice sides. Here, as a baseline the partitioning separating the Hamiltonian into mutually commuting groups of 2-local fermionic Hermitian operators is used. (c) (Spinfull) Fermi Hubbard model. In comparison with its spinless version, here the repulsive nearest neighbor coupling is replaced with a repulsive on-site spin-spin coupling. Thus it can be viewed as two spinless Hubbard models, coupled by its spin degree of freedom. Thus, it also consists of 24 lattice sides, but on a  $4 \times 3 \times 2$  graph (compare graphical legend).

(b)). For this reason we set in the following  $\mu = 0$ . Further, note that this does not make the (non-geometric) sampling problem easier as the number operators can be measured together anyway, and hence the number of "baseline" partitions is unaffected. Similarly, to the spirit of the baseline within the bosonic basis, we group here as a comparison the operators in  $H_{SpinlessHubbard}$  in groups of mutually commuting operators. For  $U \neq 0$  there are 5 groups, being 4 groups from the hopping part of the Hamiltonian with disjoint support and one group measuring the number operators. Under Jordan-Wigner mapping, this corresponds to the Pauli grouping, which is why we still call it Pauli partitioning in Figure 3.

Further, we find for  $U \approx 1$  ( $\langle \hat{N} \rangle = 8$ ), that the ground state of the model is degenerate or respectively gapless. Even though our Theorem 1 does then not strictly apply any longer, we find in this numerical test, that the sampling improvement for geometric partitioning persists.

## 6. Two-dimensional Spinful Hubbard Model

As a final example for geometric partitioning to reduce the measurement effort when estimating energies of eigenstates, we show the Hubbard model. This model, which was originally proposed as an effective model to study electron correlations, like for example how transitions from conductors to insulators occur [35], is of central importance in condensed matter physics. It resembles, the previously shown spinless fermion model, but features an on-site spin-spin (repulsive) interactions, instead of neighbor repulsion:

$$H_{\text{Hubbard}} = -t \sum_{\langle i,j \rangle, \sigma} \left( c_{i,\sigma}^\dagger c_{j,\sigma} + c_{j,\sigma}^\dagger c_{i,\sigma} \right) + U \sum_i n_{i,\uparrow} n_{i,\downarrow} - \mu \sum_{i,\sigma} n_{i,\sigma} \quad (56)$$

One can view this (spinfull) Hubbard models as two spinless ones (w.o. neighbor repulsion), that are repulsively coupled only at the same lattice sides  $i$ , forming a bi-planar graph with the two two-dimensional planes being

the up and down spin sectors. Thus, one can consider the Hubbard model as an example of geometric partitioning on a three-dimensional lattice. Testing a real three-dimensional example including cubic patches remains challenging as one would need 4 lattice sides in each dimensional direction or 64 overall.

We keep  $t = 1$  and  $\mu = 0$ , and expect again to remain close to but under half-filling for all  $U$ . Indeed for  $U \lesssim 2$  we have  $\langle \hat{N} \rangle = 10$ , which is still a larger Hilbert space than half-filling due to the particle-hole symmetry at half-filling that halves the dimension of the Hilbert subspace [36]. The baseline, we compare geometric partitioning with, works analogously to the spinless case with four partitions to measure the hopping terms and one to measure the onsite repulsion.

For the spinfull Hubbard model all three particle sectors in the middle in Figure 4 (c),  $8 \leq \langle \hat{N} \rangle \leq 10$ , and  $2.5 \lesssim U \lesssim 7.5$ , are gapless. We see that the improvement noticeably leaves the smooth trajectory it has before and after, but nonetheless and despite these cases not being captured within Theorem 1, we find the sampling improvement by geometric partitioning persists.

### E. Numerical tests of imperfect eigenstate results

Here, we give numerical examples of energy estimations of eigenstates under Haar-random noise. More explicitly, we want to motivate that the truncation of  $\mathcal{O}(2^{-n})$  is well justified in Lemma 3 (see Fig. 5 (d)). We illustrate the numerics for the resulting Corollaries 2 and 3 as well as Theorem 2 in Fig. 5 (a). The comparison in the vertical direction in Fig. 5 (a) corresponds to the sampling improvement under the effect of noise, while a comparison in horizontal direction shows improvement in noise threshold for a fixed sampling overhead  $\delta$  compared to the eigenbasis  $\mathcal{B}_H$ .

In the noiseless case, we have seen that Pauli partitions with  $|\mathcal{B}| > 2$  give larger improvements of the geometric sampling strategy or correspondingly looser numerical results compared to the derived lower bounds due to Eq. (20). This is why we chose as a test bed for our analytic unbiased noise results, the intersection between the TFIM and the TFXYM, where  $h = J = \eta = 1$  on a rectangular  $4 \times 6$  lattice.

Fig. 5 (b) shows how the expected sampling improvement  $\bar{\mathcal{G}}_{|\tilde{E}_0\rangle}(\mathcal{B}_{\text{Pauli}}, \mathcal{B}_{L_x, L_y})$  with increasing noise level as predicted by Corollary 3. The three regimes (I.) low noise, (II.) intermediate noise and (III.) noise dominated are separated with dotted lines. As predicted by Corollary 2, Eq. (32), and indicated by light/dashed/dotted cyan lines we find for (I.)  $\bar{\mathcal{G}}_{|\tilde{E}_0\rangle}(\mathcal{B}_{\text{Pauli}}, \mathcal{B}_{L_x, L_y}) \approx \mathcal{G}_{|E_0\rangle}(\mathcal{B}_{\text{Pauli}}, \mathcal{B}_{L_x, L_y})$ , for (II.)  $\bar{\mathcal{G}}_{|\tilde{E}_0\rangle}(\mathcal{B}_{\text{Pauli}}, \mathcal{B}_{L_x, L_y}) \approx 4 \text{Var}_{|E_i\rangle}(H_{\text{Pauli}}^{(1)})/(\epsilon E_0^2)$ , and for (III.)  $\bar{\mathcal{G}}_{|\tilde{E}_0\rangle}(\mathcal{B}_{\text{Pauli}}, \mathcal{B}_{L_x, L_y}) \approx \bar{\mathcal{G}}_{\epsilon=1}(\mathcal{B}_{\text{Pauli}}, \mathcal{B}_{L_x, L_y})$ .

In Fig. 5 (d), we compare the relative deviation of the expected sampling improvements as stated in Lemma 3,

where we truncated at  $\mathcal{O}(2^{-n})$  numerically with a Haar-random perturbation to the exact ground state  $|E_0\rangle$  of strength  $\epsilon$ . Consistently, the deviation is smaller for smaller  $\epsilon$ , and the maximal deviation is  $\approx 5 \cdot 10^{-4}$ , which is consistent with the dominant truncated term  $8\epsilon(1 - \epsilon) \langle O^2 \rangle / d \leq 2E_0^2/d \approx 2(2n)^2/2^n \approx 3 \cdot 10^{-4}$  in Eq. (C8). This corroborates that the applied truncation is indeed justified, and we thus focus our further discussion of the randomly perturbed case on the  $\mathcal{O}(2^{-n})$  truncated form of the variance expectation value as given in Eq. (31).

As also apparent in Figure 5 (c) for  $\epsilon \gtrsim 4 \text{Var}_{|E_i\rangle}(H_{L_x, L_y}^{(1)})/E_0^2$ , measuring in geometric partitionings becomes similarly effective as sampling in the eigenbasis. While for the noiseless case the variance in the eigenbasis is 0, it motivates for the noisy case to compare the measurement strategies with the eigenbasis as shown in Fig. 5 (c).

We already saw that geometric partitioning significantly profits from the equal distribution of energy since energy estimation in the intermediate noise regime (II.) already becomes comparable to sampling in the eigenbasis. On top, this also turns out to be beneficial for reaching a given sampling overhead  $\propto (1 + \alpha^2(\delta - \alpha^2))$ , where  $\alpha$  labels the asymmetry of energy distribution in the Pauli basis. Fig. 5 (b) shows in color the different geometric partitionings and as gray dotted lines the analytically derived expectation, see Eq. (48), where we truncated in  $\mathcal{O}(1/n)$ .

## III. DISCUSSION

The main idea we pursued in this work was to make use of the geometric locality of quantum systems to improve measurement strategies compared to sampling in Pauli bases. Conceptionally, we think of these geometrically local subsystems to be diagonalizable on the quantum hardware, meaning that the transformations mapping the eigenstates of the subsystems to the computational basis can be found. This can for instance be achieved via classical computation for small system sizes, or via known gate sequences [19]. Comparing these different measurement strategies under the optimal allocation of the sampling budget allowed us to find an sampling budget allocation agnostic cost function only in terms of the partition variances (Eq. (7)).

In our first main result, Theorem 1 together with Lemma 2, we have proven that indeed geometric partitioning always yields an advantage over Pauli partitioning for energy estimates of a system in an energy eigenstate, where we identified three cases. These are geometric partition coming from a one-dimensional cuts ( $\geq 4L$ ), two-dimensional patches ( $\geq 4L_x L_y / (L_x + L_y)$ ) or even 2-local partitions ( $\geq 4/3$ ). Typically smaller guaranteed improvements coincide with easier-to-implement measurement circuits  $U_M = U_m \otimes \dots \otimes U_m$  as block-diagonal  $U_m$  act on less qubits/lattice sites. There is something for (almost) any available measurement gate budget starting

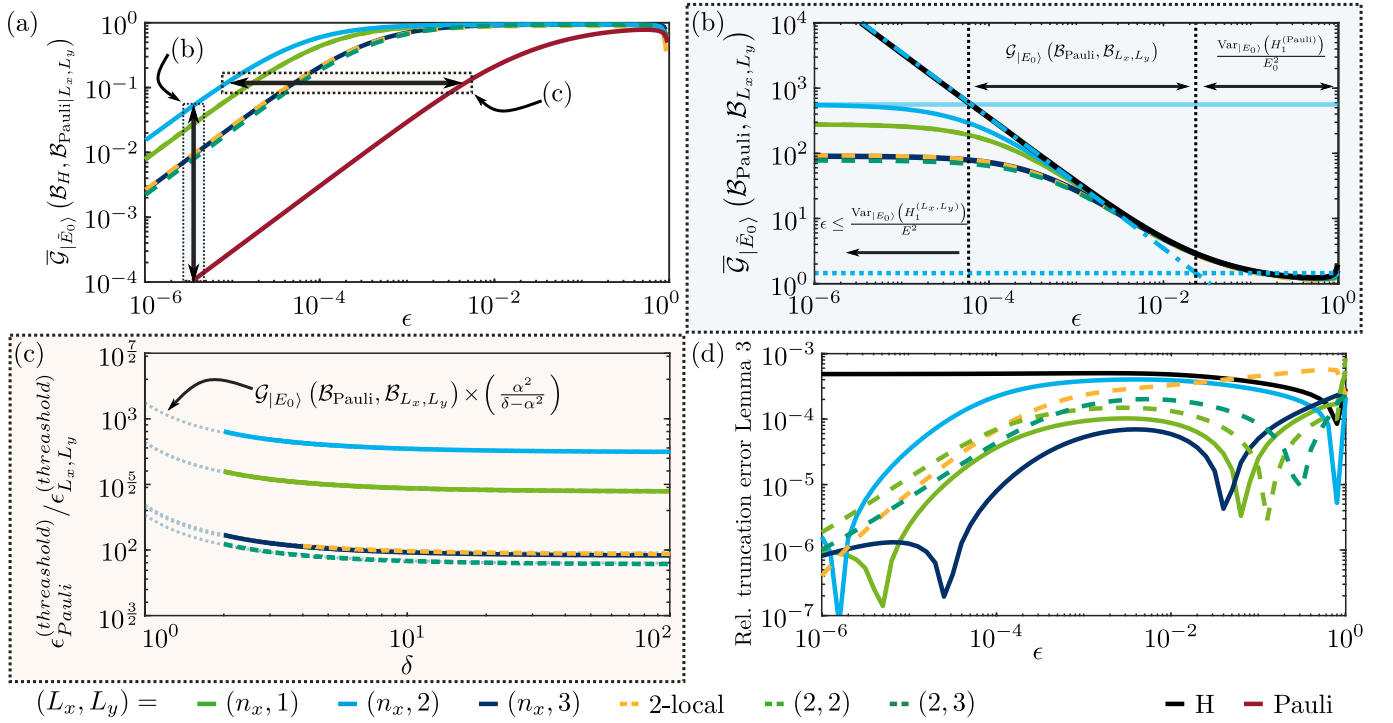


FIG. 5. **Numerical example - imperfect eigenstates.** Here we present numerical results on Lemma 3, Corollary 2 and Theorem 2. We chose the intersection of the 2D XY-model with Z field ( $\eta = 1$ ) and the 2D TFIM ( $J/h = 1$ ). As expected, we observe that larger sampling cost improvements  $\bar{\mathcal{G}}_{|E_0\rangle}(\mathcal{B}_{\text{Pauli}}, \mathcal{B}_{L_x, L_y})$  at the noise-free level also have a positive effect in the noisy case. (a) Sampling overhead of measuring in geometric or Pauli basis compared to the eigenbasis. In (b), we compare partitioning strategies for the same  $\epsilon$ , which corresponds to comparing along the vertical direction in (a). Improvements at lower noise levels already resemble the (optimal) measurement in the eigenbasis ( $\epsilon \approx 10^{-4 \dots -3}$ , also see (a)). Compare also Corollaries 2 and 3. In (c), we compare the ratios of noise thresholds for given sampling overheads  $\delta$  for geometric and Pauli partitionings, which corresponds to comparisons along horizontal arrows in (a). The prediction by Theorem. 2, Eq. (48), is shown in gray. (d) Relative error between the state vector numerics and Lemma 3, Eq. (31). For all partitions, we observe the truncation error to be  $\lesssim 5 \cdot 10^{-4}$ , which fits well to Eq. (C8), where the largest neglected (exponentially suppressed) term is  $\leq 2E_0^2/d \approx 2(2n)^2/2^n \approx 3 \cdot 10^{-4}$ .

from as little as  $n/2$  additional, potentially even mergeable, 2-qubit gates when using the 2-local geometric partitioning strategy. Twice as large partitioning blocks with e.g.  $(L_x, L_y) = (2, 2)$  then require to implement a 4-qubit measurement unitary, or worst case  $\frac{27}{4}n$  2-qubit gates [37], which appears still feasible also in near term applications. Altogether, it is a step-wise trade-off between the gate overhead implementing the block diagonal  $U_m$  and the guaranteed sampling improvement. In this trade-off, for example, 2D cuts pay off in terms of partition size as soon as  $n_x$  and  $n_y > 4L$ , as then they guarantee a better improvement for the same-sized  $U_m$  (in example light green  $L = 1$  and  $L_x = L_y = 2$  consistently performed equally well).

With our second theorem, we cover the more general case of imperfect eigenstates, perturbed by unbiased (globally Haar-random) noise, and found that the sampling complexity improvement  $\mathcal{G}$  carries over to the noisy case. Firstly, the noise strengths  $\epsilon$  above which measuring in the geometric basis effectively becomes as good as measuring in the eigenbasis is  $\propto 1/\mathcal{G}$ , meaning larger noise-free im-

provements lead to being as good as the eigenbasis down to smaller noise levels. There geometric partitions benefit again from distributing the energy equally (Corollary 2). Secondly,  $\mathcal{G}$  gives a lower limit on the noise threshold separation of geometric partitioning compared to measuring in Pauli basis to be  $\delta$ -close to sampling in the eigenbasis (Theorem 2).

Typically, more entangled or correlated states affect measurement schemes negatively [38]. In contrast to that, our ansatz here can even benefit from highly correlated states. For both 1D and 2D geometric partitionings, our Theorem 1 lower bound (cases (a) and (b)) predicts lower bounds  $\propto 1/(1 - \text{CoR}(H_{\text{cut}}, H'_{\text{cut}})) \geq 1$ . As a consequence, the guaranteed relative sampling improvement can significantly exceed  $4L$  and  $4L_x L_y / (L_x + L_y)$  for  $\text{CoR}(H_{\text{cut}}, H'_{\text{cut}}) \rightarrow 1$ . We observed this behavior featuring improvements  $\gtrsim 10^7$  for TFXYM around its oscillatory to ferromagnetic phase transition (Fig. 3 (a)). This means sampling this specific ground state  $|E_0\rangle$  once via geometric partitioning yields a similar statistic uncertainty as sampling it 10 million times via Pauli partitioning. Phe-

nomenologically, this sampling complexity improvement can be attributed to some state entanglement being disentangled via the measurement bases. In the extreme, in general inaccessible case, with rotating into the eigenbasis we would end up with a single computational state.

We focused on proving sampling improvements for geometric local models, both in bosonic and fermionic bases. We have shown in total six examples, where the geometric partitioning strategy led to an sampling improvement compared to the (Pauli) baseline, as our analysis suggested. Further, we demonstrated with the Transverse Field Biaxial Next-Nearest Neighbor Ising model, how this idea extends beyond 2-local models to a quasi-3-local one. To go forward an interesting future direction might be potentially lifting the requirement of geometric locality, and extending the idea to further types of symmetries beyond translational invariance. Similarly, we found examples of improvements beyond our lower bound, e.g. within the ferromagnetic phase  $J/h \gg 1$  of the TFIM. This motivates to investigate further more model-specific sampling improvement estimations or to exploit perturbation theory results to construct better-performing sampling basis as we provided with our Lemma 5.

Eventually, we took the stand here that we are given a perfect or unbiasedly perturbed eigenstate and aim to estimate the energy expectation value. Thus we aimed to disentangle appropriately the given state with our approach. In future work, one could flip this view around

and rather use geometric local bases as a non-variational ansatz for approximated state preparation. For instance, for ground state preparation, one could expect mostly the low-energy subspace of the geometric local bases to be relevant for the ground state of the entire system. Provided the inverses of our measurement unitaries not only lead to vanishing local energy variances but also low local energy expectation values, this strategy would support approximations with reduced effective Hilbert spaces.

## ACKNOWLEDGMENTS

This work was German Research Foundation (DFG) – Project-ID 429529648 – TRR 306 QuCoLiMa, the German Federal Ministry of Education and Research (BMBF) contract number 13N16067 “EQUAHUMO”, and Munich Quantum Valley, which is supported by the Bavarian state government with funds from the Hightech Agenda Bayern Plus. This work used resources of the Erlangen National High Performance Computing Center. T.E. acknowledges support from the International Max-Planck Research School for Physics of Light. M.K. is funded by the Fujitsu Germany GmbH as part of the endowed professorship “Quantum Inspired and Quantum Optimization.”

- 
- [1] J. Haah, A. W. Harrow, Z. Ji, X. Wu, and N. Yu, Sample-optimal tomography of quantum states, *IEEE Transactions on Information Theory* **63**, 5628 (2017).
- [2] S. Arunachalam and R. De Wolf, Optimal quantum sample complexity of learning algorithms, *Journal of Machine Learning Research* **19**, 1 (2018).
- [3] R. Takagi, H. Tajima, and M. Gu, Universal sampling lower bounds for quantum error mitigation, *Physical Review Letters* **131**, 210602 (2023).
- [4] P. Gokhale, O. Angiuli, Y. Ding, K. Gui, T. Tomesh, M. Suchara, M. Martonosi, and F. T. Chong, Minimizing state preparations in variational quantum eigensolver by partitioning into commuting families, [arXiv:1907.13623 \[quant-ph\]](https://arxiv.org/abs/1907.13623) (2019).
- [5] A. Jena, S. Genin, and M. Mosca, Pauli partitioning with respect to gate sets, [arXiv:1907.07859 \[quant-ph\]](https://arxiv.org/abs/1907.07859).
- [6] V. Verteletskyi, T.-C. Yen, and A. F. Izmaylov, Measurement optimization in the variational quantum eigensolver using a minimum clique cover, *J. Chem. Phys.* **152**, 124114 (2020), [arXiv:1907.03358 \[quant-ph\]](https://arxiv.org/abs/1907.03358).
- [7] W. J. Huggins, J. R. McClean, N. C. Rubin, Z. Jiang, N. Wiebe, K. B. Whaley, and R. Babbush, Efficient and noise resilient measurements for quantum chemistry on near-term quantum computers, *npj Quantum Information* **7**, 1 (2021).
- [8] A. Gresch and M. Kliesch, Guaranteed efficient energy estimation of quantum many-body Hamiltonians using ShadowGrouping, [arXiv:2301.03385 \[quant-ph\]](https://arxiv.org/abs/2301.03385) (2023).
- [9] H.-Y. Huang, R. Kueng, and J. Preskill, Predicting many properties of a quantum system from very few measurements, *Nature Physics* **16**, 1050 (2020).
- [10] C. Hadfield, S. Bravyi, R. Raymond, and A. Mezzacapo, Measurements of quantum Hamiltonians with locally-biased classical shadows, [arXiv:2006.15788 \[quant-ph\]](https://arxiv.org/abs/2006.15788) (2020).
- [11] C. Hadfield, Adaptive Pauli shadows for energy estimation, [arXiv:2105.12207 \[quant-ph\]](https://arxiv.org/abs/2105.12207).
- [12] A. Elben, S. T. Flammia, H.-Y. Huang, R. Kueng, J. Preskill, B. Vermersch, and P. Zoller, The randomized measurement toolbox, *Nat. Rev. Phys.* **5**, 9 (2022), [arXiv:2203.11374](https://arxiv.org/abs/2203.11374).
- [13] R. Brieger, M. Heinrich, I. Roth, and M. Kliesch, Stability of classical shadows under gate-dependent noise, [arXiv:2310.19947 \[quant-ph\]](https://arxiv.org/abs/2310.19947) (2023).
- [14] O. Crawford, B. van Straaten, D. Wang, T. Parks, E. Campbell, and S. Brierley, Efficient quantum measurement of pauli operators in the presence of finite sampling error, *Quantum* **5**, 385 (2021).
- [15] A. Chatterjee, P. Stevenson, S. De Franceschi, A. Morello, N. P. de Leon, and F. Kuemmeth, Semiconductor qubits in practice, *Nature Reviews Physics* **3**, 157 (2021).
- [16] G. Burkard, T. D. Ladd, A. Pan, J. M. Nichol, and J. R. Petta, Semiconductor spin qubits, *Reviews of Modern Physics* **95**, 025003 (2023).
- [17] F. Arute, K. Arya, R. Babbush, D. Bacon, J. C. Bardin, R. Barends, R. Biswas, S. Boixo, F. G. S. L. Brandao, D. A. Buell, B. Burkett, Y. Chen, Z. Chen, B. Chiaro, R. Collins, W. Courtney, A. Dunsworth,



- E. Farhi, B. Foxen, A. Fowler, C. Gidney, M. Giustina, R. Graff, K. Guerin, S. Habegger, M. P. Harrigan, M. J. Hartmann, A. Ho, M. Hoffmann, T. Huang, T. S. Humble, S. V. Isakov, E. Jeffrey, Z. Jiang, D. Kafri, K. Kechedzhi, J. Kelly, P. V. Klimov, S. Knysh, A. Korotkov, F. Kostritsa, D. Landhuis, M. Lindmark, E. Lucero, D. Lyakh, S. Mandrà, J. R. McClean, M. McEwen, A. Megrant, X. Mi, K. Michielsen, M. Mohseni, J. Mutus, O. Naaman, M. Neeley, C. Neill, M. Y. Niu, E. Ostby, A. Petukhov, J. C. Platt, C. Quintana, E. G. Rieffel, P. Roushan, N. C. Rubin, D. Sank, K. J. Satzinger, V. Smelyanskiy, K. J. Sung, M. D. Trevithick, A. Vainsencher, B. Villalonga, T. White, Z. J. Yao, P. Yeh, A. Zalcman, H. Neven, and J. M. Martinis, Quantum supremacy using a programmable superconducting processor, *Nature* **574**, 505 (2019).
- [18] A. Blais, A. L. Grimsmo, S. M. Girvin, and A. Wallraff, Circuit quantum electrodynamics, *Reviews of Modern Physics* **93**, 025005 (2021).
- [19] F. Verstraete, J. I. Cirac, and J. I. Latorre, Quantum circuits for strongly correlated quantum systems, *Physical Review A* **79**, 032316 (2009).
- [20] H. P. Robertson, The uncertainty principle, *Physical Review* **34**, 163 (1929).
- [21] M. B. Hastings and T. Koma, Spectral gap and exponential decay of correlations, *Communications in mathematical physics* **265**, 781 (2006).
- [22] M. Henkel, Statistical mechanics of the 2d quantum xy model in a transverse field, *Journal of Physics A: Mathematical and General* **17**, L795 (1984).
- [23] Y. Nishiyama, Multicritical behavior of the fidelity susceptibility for the 2d quantum transverse-field xy model, *The European Physical Journal B* **92**, 1 (2019).
- [24] E. Ising, *Beitrag zur Theorie des Ferro-und Paramagnetismus*, Ph.D. thesis, Hamburgische Universität (1924).
- [25] L. Onsager, Crystal statistics. i. a two-dimensional model with an order-disorder transition, *Physical Review* **65**, 117 (1944).
- [26] T. D. Schultz, D. C. Mattis, and E. H. Lieb, Two-dimensional ising model as a soluble problem of many fermions, *Reviews of Modern Physics* **36**, 856 (1964).
- [27] H. W. J. Blöte and Y. Deng, Cluster monte carlo simulation of the transverse Ising model, *Phys. Rev. E* **66**, 066110 (2002).
- [28] R. Hornreich, R. Liebmann, H. Schuster, and W. Selke, Lifshitz points in Ising systems, *Zeitschrift für Physik B Condensed Matter* **35**, 91 (1979).
- [29] T. Eckstein, R. Mansuroglu, P. Czarnik, J.-X. Zhu, M. J. Hartmann, L. Cincio, A. T. Sornborger, and Z. Holmes, Large-scale simulations of floquet physics on near-term quantum computers, *npj Quantum Information* **10**, 84 (2024).
- [30] V. Murg, F. Verstraete, and J. I. Cirac, Variational study of hard-core bosons in a two-dimensional optical lattice using projected entangled pair states, *Physical Review A—Atomic, Molecular, and Optical Physics* **75**, 033605 (2007).
- [31] J. Jordan, R. Orús, and G. Vidal, Numerical study of the hard-core bose-hubbard model on an infinite square lattice, *Phys. Rev. B* **79**, 174515 (2009).
- [32] H. A. Gersch and G. C. Knollman, Quantum cell model for bosons, *Physical Review* **129**, 959 (1963).
- [33] Y. Yanay, J. Braumüller, S. Gustavsson, W. D. Oliver, and C. Tahan, Two-dimensional hard-core bose-hubbard model with superconducting qubits, *npj Quantum Information* **6**, 58 (2020).
- [34] N. Zhang and C. Henley, Stripes and holes in a two-dimensional model of spinless fermions or hardcore bosons, *Phys. Rev. B* **68**, 014506 (2003).
- [35] J. Hubbard, Electron correlations in narrow energy bands, *Proceedings of the Royal Society of London. Series A. Mathematical and Physical Sciences* **276**, 238 (1963).
- [36] E. H. Lieb, Two theorems on the hubbard model, *Physical review letters* **62**, 1201 (1989).
- [37] A. Barenco, C. H. Bennett, R. Cleve, D. P. DiVincenzo, N. Margolus, P. Shor, T. Sleator, J. A. Smolin, and H. Weinfurter, Elementary gates for quantum computation, *Physical review A* **52**, 3457 (1995).
- [38] A. Anshu, Concentration bounds for quantum states with finite correlation length on quantum spin lattice systems, *New Journal of Physics* **18**, 083011 (2016).
- [39] M. Kliesch and I. Roth, Theory of quantum system certification, *PRX Quantum* **2**, 010201 (2021), tutorial, [arXiv:2010.05925 \[quant-ph\]](https://arxiv.org/abs/2010.05925).

### Appendix A: How to compare measurement strategies

A measurement strategy in quantum mechanics has the aim of determining an estimator for the true observable expectation value  $\langle \psi | H | \psi \rangle$  as accurate as possible with a given number of measurements  $M$ . Then standard deviation of an unbiased estimator is given by:

$$\frac{1}{M} \Delta H^2 = \frac{1}{M} \text{Var}_{|\psi\rangle}(H) \quad (\text{A1})$$

Realizing this sampling error requires the ability to measure observable  $H$  at once. However, finding the eigenbasis, in which one would need to measure, generally cannot be done in polynomial time, as we need to diagonalize the entire exponentially large Hilbert space to map  $|\psi\rangle$  into the eigenbasis of  $H$ , in the worst case. Thus, in typical non-trivial sampling tasks, one needs to split  $H$  into parts  $H_b$  of which the transformations into their respective eigenbasis are known, such that  $H = \sum_{H_b \in \mathcal{B}} H_b$  with partitioning  $\mathcal{B}$ . Then the measurement error can be upper bounded by (step by step calculation of Eq. (7)):

$$\begin{aligned} \frac{1}{M} \Delta H^2 &= \frac{1}{M} \left[ \sum_{H_b \in \mathcal{B}} \text{Var}_{|\psi\rangle}(H_b) + \sum_{\substack{H_b, H'_b \in \mathcal{B} \\ H_b \neq H'_b}} \text{CoV}_{|\psi\rangle}(H_b, H'_b) \right] \leq \frac{1}{M} \left[ \sum_{H_b \in \mathcal{B}} \text{Var}_{|\psi\rangle}(H_b) + \sum_{\substack{H_b, H'_b \in \mathcal{B} \\ H_b \neq H'_b}} |\text{CoV}_{|\psi\rangle}(H_b, H'_b)| \right] \\ &\leq \frac{1}{M} \left[ \sum_{H_b \in \mathcal{B}} \text{Var}_{|\psi\rangle}(H_b) + \sum_{\substack{H_b, H'_b \in \mathcal{B} \\ H_b \neq H'_b}} \sqrt{\text{Var}_{|\psi\rangle}(H_b) \text{Var}_{|\psi\rangle}(H'_b)} \right] = \frac{1}{M} \left[ \sum_{H_b \in \mathcal{B}} \sqrt{\text{Var}_{|\psi\rangle}(H_b)} \right]^2 \leq \sum_{H_b \in \mathcal{B}} \frac{\text{Var}_{|\psi\rangle}(H_b)}{M_b} \end{aligned} \quad (\text{A2})$$

where  $M = \sum_{b=1}^{|\mathcal{B}|} M_b$ . The first inequality adds absolute values to the covariances and the second inequality is the Cauchy-Schwarz inequality. Using Lagrangian multipliers, one finds that the last inequality becomes an equality precisely for the optimal distribution of sampling budget  $M$ . Let us write this down explicitly. The Lagrangian is given by:

$$\mathcal{L}(\vec{M}, \lambda) := \sum_{b=1}^{|\mathcal{B}|} \frac{\text{Var}_{|\psi\rangle}(H_b)}{M_b} - \lambda \left( M - \sum_{b=1}^{|\mathcal{B}|} M_b \right) \quad (\text{A3})$$

where we named  $\vec{M}$  being a vector of all  $M_b$ . Then the stationary conditions yields:

$$0 \stackrel{!}{=} \frac{\partial \mathcal{L}(\vec{M}, \lambda)}{\partial M_b} = -\frac{\text{Var}_{|\psi\rangle}(H_b)}{M_b^2} + \lambda \quad \forall b \in \{1, 2, \dots, B\} \quad (\text{A4})$$

$$0 \stackrel{!}{=} \frac{\partial \mathcal{L}(\vec{M}, \lambda)}{\partial \lambda} = M - \sum_{b=1}^B M_b \quad (\text{A5})$$

As  $\text{Var}_{|\psi\rangle}(H_b) \geq 0$ , we know that  $\lambda = \text{Var}_{|\psi\rangle}(H_b)/M_b^2 \geq 0$ , and in order to minimize the standard error,  $M_b$  needs to be chosen such that all  $\sqrt{\text{Var}_{|\psi\rangle}(H_b)}/M_b$  become equal. This allows us to express  $\lambda$  in terms of  $M$  and  $\text{Var}_{|\psi\rangle}(H_b)$ :

$$M = \sum_{b=1}^{|\mathcal{B}|} M_b = \sum_{b=1}^{|\mathcal{B}|} \sqrt{\frac{\text{Var}_{|\psi\rangle}(H_b)}{\lambda}} \Rightarrow \sqrt{\lambda} = \frac{1}{M} \sum_{b=1}^{|\mathcal{B}|} \sqrt{\text{Var}_{|\psi\rangle}(H_b)} \quad (\text{A6})$$

Then Eq. (A6) and Eq. (A4) solve the constraint minimization problem:

$$\min_{M = \sum M_b} \left( \sum_{H_b \in \mathcal{B}} \frac{\text{Var}_{|\psi\rangle}(H_b)}{M_b} \right) = \sum_{H_b \in \mathcal{B}} \sqrt{\text{Var}_{|\psi\rangle}(H_b)} \sqrt{\lambda} = \frac{1}{M} \left[ \sum_{H_b \in \mathcal{B}} \sqrt{\text{Var}_{|\psi\rangle}(H_b)} \right]^2 \quad (\text{A7})$$

$\text{Var}_{|\psi\rangle}(H_b)$  are the sampling errors we will experience when measuring  $H$  in the partitioning  $\mathcal{B}$ . The partitioning  $\mathcal{B}$  is by no means unique. Rather it gives us a way to compare sampling budget allocation agnostic sampling strategies by comparing  $[\sum_{H_b \in \mathcal{B}} \sqrt{\text{Var}_{|\psi\rangle}(H_b)}]^2$ , motivation our relative sampling complexity cost function in Definition 1.

In a more general setting, where we are interested to upper bound the (average) measurement error, not only w.r.t. a single state  $|\psi\rangle$ , but w.r.t. to an assemble of states  $|\tilde{\psi}\rangle$ , we need to consider the expectation value over  $|\tilde{\psi}\rangle$ :

$$\frac{1}{M} \overline{\Delta H^2} = \frac{1}{M} \mathbb{E} \left[ \text{Var}_{|\tilde{\psi}\rangle}(H) \right] \quad (\text{A8})$$

Applying once more the Cauchy-Schwarz inequality, this time on the expectation value over  $|\tilde{\psi}\rangle$ , as well as using linearity of the expectation value, we can obtain a similar upper bound to Eq. (A2):

$$\begin{aligned} \frac{1}{M} \overline{\Delta H^2} &= \frac{1}{M} \mathbb{E} \left[ \text{Var}_{|\tilde{\psi}\rangle}(H) \right] \leq \frac{1}{M} \mathbb{E} \left[ \left[ \sum_{H_b \in \mathcal{B}} \sqrt{\text{Var}_{|\psi\rangle}(H_b)} \right]^2 \right] \\ &= \frac{1}{M} \mathbb{E} \left[ \sum_{H_b \in \mathcal{B}} \text{Var}_{|\psi\rangle}(H_b) \right] + \frac{1}{M} \mathbb{E} \left[ \sum_{H'_b \neq H_b \in \mathcal{B}} \sqrt{\text{Var}_{|\psi\rangle}(H_b)} \sqrt{\text{Var}_{|\psi\rangle}(H'_b)} \right] \\ &\leq \frac{1}{M} \sum_{H_b \in \mathcal{B}} \mathbb{E} [\text{Var}_{|\psi\rangle}(H_b)] + \frac{1}{M} \sum_{H'_b \neq H_b \in \mathcal{B}} \sqrt{\mathbb{E} [\text{Var}_{|\psi\rangle}(H_b)]} \sqrt{\mathbb{E} [\text{Var}_{|\psi\rangle}(H'_b)]} \\ &= \frac{1}{M} \left[ \sum_{H_b \in \mathcal{B}} \sqrt{\mathbb{E} [\text{Var}_{|\psi\rangle}(H_b)]} \right]^2 \end{aligned} \quad (\text{A9})$$

## Appendix B: Sample Improvements (Proof of Theorem 1)

We can write the horizontal interactions as an orbit of the translation group acting on a unit cell Hamiltonian  $V$

$$H_2^h = \sum_{\ell=1}^{n_x} \sum_{m=1}^{n_y} T_m^y T_\ell^x V T_{-\ell}^x T_{-m}^y, \quad (\text{B1})$$

and the vertical interactions accordingly

$$H_2^v = S H_2^h S. \quad (\text{B2})$$

We begin with a proof of strategy (c), which requires  $L_x, L_y > 2$ . The sample improvement reads

$$\mathcal{G}_{|E_0\rangle}(\mathcal{B}_{\text{Pauli}}, \mathcal{B}_{L_x, L_y}) = \frac{\text{Var}(H_2)}{\text{Var}\left(\frac{1}{2}(H - H_{\text{cut}}^x - H_{\text{cut}}^y + H_{\text{cut}}^{x'} + H_{\text{cut}}^{y'})\right)}, \quad (\text{B3})$$

since on eigenstates  $\text{Var}(H_2) = \text{Var}(H_1)$  and

$$\begin{aligned} \text{Var}\left(\frac{1}{2}(H - H_{\text{cut}}^x - H_{\text{cut}}^y + H_{\text{cut}}^{x'} + H_{\text{cut}}^{y'})\right) &= \text{Var}\left(\frac{1}{2}(H + H_{\text{cut}}^x + H_{\text{cut}}^y - H_{\text{cut}}^{x'} - H_{\text{cut}}^{y'})\right) \\ &= \frac{1}{4} \text{Var}\left(H_{\text{cut}}^x + H_{\text{cut}}^y - H_{\text{cut}}^{x'} - H_{\text{cut}}^{y'}\right). \end{aligned} \quad (\text{B4})$$

Let us consider numerator and denominator separately. First, observe that  $\text{Var}(H_2) = 2 \text{Var}(H_2^h) + 2 \text{Var}(S H_2^h)$  from invariance of the ground state. Further, we can express both terms in terms of covariances. We have

$$\text{Var}(H_2^h) = \text{Var}\left(\sum_{\ell=1}^{n_x} \sum_{m=1}^{n_y} T_m^y T_\ell^x V T_{-\ell}^x T_{-m}^y\right) = n_x n_y \sum_{\ell=1}^{n_x} \sum_{m=1}^{n_y} \text{Var}(T_m^y T_\ell^x V), \quad (\text{B5})$$

where we used the multilinearity of the covariance, the fact that translation operators commute,  $[T_\ell^x, T_m^y] = 0$ , and again symmetry of the ground state to identify  $n_x n_y$  identical terms. Similarly, we can calculate

$$\text{Var}(S H_2^h) = n_x n_y \sum_{\ell=1}^{n_x} \sum_{m=1}^{n_y} \text{Var}(S T_m^y T_\ell^x V). \quad (\text{B6})$$

Let us separate the qubit number  $n = n_x n_y$  from the correlators and write  $\text{Var}(H_2) =: 2nC_1$ . The denominator can be treated in a similar way.

$$\begin{aligned} & \text{Var}(H_{cut}^x + H_{cut}^y - H_{cut}^{x'} - H_{cut}^{y'}) \\ &= 2 \text{Var}(H_{cut}^x) + 2 \text{Var}(H_{cut}^y) - \text{Var}(T_1^x H_{cut}^x) - \text{Var}(T_{-1}^x H_{cut}^x) - \text{Var}(T_1^y H_{cut}^y) - \text{Var}(T_{-1}^y H_{cut}^y) \end{aligned} \quad (\text{B7})$$

Expressing  $H_{cut}^x$  in terms of  $V$ , we calculate

$$\text{Var}(H_{cut}^x) = \text{Var} \left( \sum_{\ell=1}^{n_x/L_x} \sum_{m=1}^{n_y} T_{\ell L_x}^x T_m^y V T_{-m}^y T_{-\ell L_x}^x \right) = n_y \frac{n_x}{L_x} \sum_{\ell=1}^{n_x/L_x} \sum_{m=1}^{n_y} \text{Var}(T_{\ell L_x}^x T_m^y V). \quad (\text{B8})$$

and similarly

$$\text{Var}(H_{cut}^y) = n_x \frac{n_y}{L_y} \sum_{m=1}^{n_y/L_y} \sum_{\ell=1}^{n_x} \text{Var}(T_{m L_y}^y T_{\ell}^x S V) \quad (\text{B9})$$

$$\text{Var}(T_1^x H_{cut}^x) = n_y \frac{n_x}{L_x} \sum_{\ell=1}^{n_x/L_x} \sum_{m=1}^{n_y} \text{Var}(T_{\ell L_x+1}^x T_m^y V) \quad (\text{B10})$$

$$\text{Var}(T_{-1}^x H_{cut}^x) = n_y \frac{n_x}{L_x} \sum_{\ell=1}^{n_x/L_x} \sum_{m=1}^{n_y} \text{Var}(T_{\ell L_x-1}^x T_m^y V) \quad (\text{B11})$$

$$\text{Var}(T_1^y H_{cut}^y) = n_x \frac{n_y}{L_y} \sum_{m=1}^{n_y/L_y} \sum_{\ell=1}^{n_x} \text{Var}(T_{m L_y+1}^y T_{\ell}^x S V). \quad (\text{B12})$$

Separating qubit number and cluster length, we write  $\text{Var}(H_{cut}^x + H_{cut}^y - H_{cut}^{x'} - H_{cut}^{y'}) = 2 \left( \frac{n}{L_x} C_2^x + \frac{n}{L_y} C_2^y \right)$  and altogether

$$\mathcal{G}_{|E_i\rangle}(\mathcal{B}_{\text{Pauli}}, \mathcal{B}_{L_x, L_y}) = 4L_x L_y \frac{C_1}{L_y C_2^x + L_x C_2^y}, \quad (\text{B13})$$

with the system dependent constants

$$C_1 = \sum_{\ell=1}^{n_x} \sum_{m=1}^{n_y} \text{Var}(T_m^y T_{\ell}^x V) + \sum_{\ell=1}^{n_x} \sum_{m=1}^{n_y} \text{Var}(S T_m^y T_{\ell}^x V) \quad (\text{B14})$$

$$C_2^x = \sum_{\ell=1}^{n_x/L_x} \sum_{m=1}^{n_y} \left( \text{Var}(T_{\ell L_x}^x T_m^y V) - \frac{1}{2} \text{Var}(T_{\ell L_x+1}^x T_m^y V) - \frac{1}{2} \text{Var}(T_{\ell L_x-1}^x T_m^y V) \right) \quad (\text{B15})$$

$$C_2^y = \sum_{m=1}^{n_y/L_y} \sum_{\ell=1}^{n_x} \left( \text{Var}(T_{m L_y}^y T_{\ell}^x S V) - \frac{1}{2} \text{Var}(T_{m L_y+1}^y T_{\ell}^x S V) - \frac{1}{2} \text{Var}(T_{m L_y-1}^y T_{\ell}^x S V) \right). \quad (\text{B16})$$

From  $C_2^x \leq C_1$  and  $C_2^y \leq C_1$ , we already have  $\mathcal{G}_{|E_i\rangle}(\mathcal{B}_{\text{Pauli}}, \mathcal{B}_{L_x, L_y}) \geq \frac{4L_x L_y}{L_x + L_y}$  as a lower bound which can be further improved as follows:

$$H_{cut} := H_{cut}^x + H_{cut}^y \quad H'_{cut} := H_{cut}^{x'} + H_{cut}^{y'} \quad (\text{B17})$$

Then we have similarly to before:

$$H_{cut} = T_{-1}^y T_{-1}^x H'_{cut} T_1^y T_1^x \quad \Rightarrow \quad \text{Var}(H_{cut}) = \text{Var}(H'_{cut}) \quad (\text{B18})$$

due to the translational invariance of the eigenstate. Thus, we can write the denominator as

$$\text{Var}(H_{cut}^x + H_{cut}^y - H_{cut}^{x'} - H_{cut}^{y'}) = \text{Var}(H_{cut} - H'_{cut}) = \text{Var}(H_{cut}) + \text{Var}(H'_{cut}) - 2\text{CoV}(H_{cut}, H'_{cut}) \quad (\text{B19})$$

$$= 2 \text{Var}(H_{cut}) \left[ 1 - \frac{\text{CoV}(H_{cut}, H'_{cut})}{\sqrt{\text{Var}(H_{cut})} \sqrt{\text{Var}(H'_{cut})}} \right] \quad (\text{B20})$$

$$= 2 \text{Var}(H_{cut}) \left[ 1 - \text{CoR}(H_{cut}, H'_{cut}) \right] \quad (\text{B21})$$



Again due to the translational symmetry of  $|E_i\rangle$  we have

$$\text{CoV}(H_{cut}, H'_{cut}) = \text{CoV}(H_{cut}, T_{-1}^y T_{-1}^x H_{cut} T_1^y T_1^x) = \text{CoV}(T_{-1}^x T_{-1}^y H_{cut}, T_{-1}^y T_{-1}^x H_{cut}) \quad (\text{B22})$$

$$= \text{Var}(T_{-1}^x T_{-1}^y H_{cut}) \geq 0 \quad (\text{B23})$$

From a similar calculation we have  $\text{Var}(H_{cut}) = \text{Var}(H_{cut}^x + H_{cut}^y) = \text{Var}(H_{cut}^x) + \text{Var}(H_{cut}^y) + 2\text{CoV}(H_{cut}^x, H_{cut}^y) \leq \text{Var}(H_{cut}^x) + \text{Var}(H_{cut}^y)$

$$\mathcal{G}_{|E_0\rangle}(\mathcal{B}_{\text{Pauli}}, \mathcal{B}_{L_x, L_y}) = 4 \frac{\text{Var}(H_2)}{2 \text{Var}(H_{cut})} \frac{1}{1 - \text{CoR}(H_{cut}, H'_{cut})} \quad (\text{B24})$$

$$\geq 4 \frac{2nC_1}{2 \text{Var}(H_{cut}^x) + 2 \text{Var}(H_{cut}^y)} \frac{1}{1 - \text{CoR}(H_{cut}, H'_{cut})} \quad (\text{B25})$$

$$= 4 \frac{2nC_1}{2 \left( \frac{n}{L_x} C_2^x + \frac{n}{L_y} C_2^y \right)} \frac{1}{1 - \text{CoR}(H_{cut}, H'_{cut})} \quad (\text{B26})$$

$$\geq 4 \frac{L_x L_y}{L_x + L_y} \frac{1}{1 - \text{CoR}(H_{cut}, H'_{cut})} \quad (\text{B27})$$

◇

For strategy (a), we set  $L_x = n_x$  and call  $L_y =: L$ . The sample improvement reads

$$\mathcal{G}_{|E_0\rangle}(\mathcal{B}_{\text{Pauli}}, \mathcal{B}_{L_x, L_y}) = 4 \frac{\text{Var}(H_2)}{\text{Var}(H_{cut} - H'_{cut})}. \quad (\text{B28})$$

While the numerator is the same as before, the denominator becomes  $\text{Var}(H_{cut} - H'_{cut}) = 2(\text{Var}(H_{cut}) - \text{Var}(T_1^y H_{cut}))$ , cf. Eq. (B7). We can further simplify Eq. (B5) in case (a) to be

$$\text{Var}(H_2^h) = L \sum_{m=1}^L \text{Var}(T_m^y H_{cut}). \quad (\text{B29})$$

Altogether we have

$$\mathcal{G}_{|E_0\rangle}(\mathcal{B}_{\text{Pauli}}, \mathcal{B}_{L_x, L_y}) \geq 4L \frac{\sum_{m=1}^L \text{Var}(T_m^y H_{cut})}{\text{Var}(H_{cut}) - \text{Var}(T_1^y H_{cut})} \geq 4L \frac{1}{1 - \frac{\text{Var}(T_1^y H_{cut})}{\text{Var}(H_{cut})}} = 4L \frac{1}{1 - \text{CoR}(H_{cut}, H'_{cut})}, \quad (\text{B30})$$

where we dropped the positive term  $\text{Var}(SH_2^h)$  in the first step. For  $L \geq 2$  we even have:

$$\mathcal{G}_{|E_0\rangle}(\mathcal{B}_{\text{Pauli}}, \mathcal{B}_{L_x, L_y}) \geq 4L \frac{1 + \frac{\text{Var}(T_1^y H_{cut})}{\text{Var}(H_{cut})}}{1 - \frac{\text{Var}(T_1^y H_{cut})}{\text{Var}(H_{cut})}} = 4L \frac{1 + \text{CoR}(H_{cut}, H'_{cut})}{1 - \text{CoR}(H_{cut}, H'_{cut})}, \quad (\text{B31})$$

◇

At last, strategy (b) assumes minimal clusters of  $L_x = 1$  and  $L_y = 2$  and vice versa. A 2-local Hamiltonian has to be split into four parts, which do not commute in general,  $H = H_A^x + H_B^x + H_A^y + H_B^y$ . For higher locality, the following discussion can be straight-forwardly generalized. Since the four terms are connected by symmetry under translations and local rotations exchanging  $x$  and  $y$ ,  $H_A^x = T_1^x H_B^x T_{-1}^x = SH_A^y S = T_1^x SH_B^y ST_{-1}^x$ , their variances coincides. As a result, the sample improvement again becomes very simple

$$\mathcal{G}_{|E_0\rangle}(\mathcal{B}_{\text{Pauli}}, \mathcal{B}_{L_x, L_y}) = \left[ \frac{\sqrt{\text{Var}(H_1)} + \sqrt{\text{Var}(H_2)}}{\sqrt{\text{Var}(H_A^x)} + \sqrt{\text{Var}(H_B^x)} + \sqrt{\text{Var}(H_A^y)} + \sqrt{\text{Var}(H_B^y)}} \right]^2 = \frac{1}{4} \frac{\text{Var}(H_2)}{\text{Var}(H_A^x)}. \quad (\text{B32})$$

We can use  $\text{Var}(H_2)$  from before and calculate the remaining variance of  $H_A^x = H_I + \frac{1}{4}H_1 = H_I + \frac{1}{4}(H - H_2)$ , with the interactions  $H_I = \sum_{\ell=1}^{n_x/2} \sum_{m=1}^{n_y} T_{2\ell}^x T_m^y V T_{-m}^y T_{-2\ell}^x$ . The variance of  $H_A^x$  can be calculated via  $\text{Var}(H_A^x) = \text{Var}(O) + \frac{1}{16} \text{Var}(H_2) - \frac{1}{4}(\text{Cov}(O, H_2) + \text{Cov}(H_2, O))$ . Using the same methods as before, we calculate

$$\text{Var}(H_I) = n_y \frac{n_x}{2} \sum_{\ell=1}^{n_x/2} \sum_{m=1}^{n_y} \text{Var}(T_{2\ell}^x T_m^y V), \quad (\text{B33})$$

which is only the first term of  $C_2^x$  from Eq. (B15). We separate the factor  $\frac{n}{2}$  and define the remainder of Eq. (B33) a new constant  $C_3$ . Similarly, the covariance reads

$$\text{Cov}(O, H_2) = n_y \frac{n_x}{2} \sum_{\ell=1}^{n_x} \sum_{m=1}^{n_y} \text{Cov}(V, T_\ell^x T_m^y V + T_\ell^x T_m^y S V) = \frac{n}{2} C_1 = \text{Cov}(H_2, O) \quad (\text{B34})$$

Altogether we obtain

$$\mathcal{G}_{|E_0\rangle}(\mathcal{B}_{\text{Pauli}}, \mathcal{B}_{L_x, L_y}) = \frac{1}{4} \frac{2nC_1}{\frac{n}{2}C_3 + \frac{n}{8}C_1 - \frac{n}{4}C_1} = \frac{C_1}{C_3 - \frac{1}{4}C_1} \geq \frac{4}{3}, \quad (\text{B35})$$

since  $C_1 \geq C_3$ . □

### Appendix C: Variance of isotropically perturbed states (Proof of Lemma 3)

We will use the flip operator defined by

$$\mathbb{F} |\psi_1\rangle |\psi_2\rangle := |\psi_2\rangle |\psi_1\rangle, \quad (\text{C1})$$

the so-called swap-trick (e.g. see [39, Eq. (7)])

$$\text{Tr}[AB] = \text{Tr}[(A \otimes B)\mathbb{F}], \quad (\text{C2})$$

and that (e.g. see [39, Eq. (163)])

$$\begin{aligned} \mathbb{E} |\xi\rangle &= 0, & \mathbb{E} |\xi\rangle \langle \xi| \langle \xi| &= 0, \\ \mathbb{E} |\xi\rangle \langle \xi| &= \mathbf{1}/d, & \mathbb{E} |\xi\rangle \langle \xi|^{\otimes 2} &= \frac{1}{d(d+1)} (\mathbf{1} + \mathbb{F}). \end{aligned} \quad (\text{C3})$$

Note that the last equality implies

$$\mathbb{E} [\langle \xi | O | \xi \rangle^2] = \mathbb{E} \text{Tr}[\langle \xi | \langle \xi |^{\otimes 2} O^{\otimes 2} \mathbb{F}] = \frac{1}{d(d+1)} (\text{Tr}[O^{\otimes 2} \mathbb{F}^2] + \text{Tr}[O^{\otimes 2} \mathbb{F}]) = \frac{\text{Tr}[O]^2 + \|O\|_F^2}{d(d+1)}. \quad (\text{C4})$$

Since  $\text{Var}(O) = \text{Var}(O + \lambda \mathbf{1})$  we assume w.l.o.g. that  $\text{Tr}[O] = 0$ . With these preliminaries, we then verify the claimed identity by a straightforward calculation,

$$\begin{aligned} \mathbb{E} \text{Var}_{|\tilde{\psi}\rangle}(O) &= \mathbb{E} [\langle \tilde{\psi} | O^2 | \tilde{\psi} \rangle - \langle \tilde{\psi} | O | \tilde{\psi} \rangle^2] = (1 - \epsilon) \langle \psi | O^2 | \psi \rangle + \epsilon \mathbb{E} [\langle \xi | O^2 | \xi \rangle] - (1 - \epsilon)^2 \langle \psi | O | \psi \rangle^2 \\ &\quad - \epsilon^2 \mathbb{E} [\langle \xi | O | \xi \rangle^2] - 4\epsilon(1 - \epsilon) \mathbb{E} [\langle \psi | O | \xi \rangle \langle \xi | O | \psi \rangle] - 2\epsilon(1 - \epsilon) \langle \psi | O | \psi \rangle \mathbb{E} [\langle \xi | O | \xi \rangle] \end{aligned} \quad (\text{C5})$$

$$\begin{aligned} &= (1 - \epsilon) \langle \psi | O^2 | \psi \rangle + \epsilon \text{Tr}[O^2 \mathbb{E} |\xi\rangle \langle \xi|] - (1 - \epsilon)^2 \langle \psi | O | \psi \rangle^2 - \epsilon^2 \mathbb{E} [\langle \xi | O | \xi \rangle^2] \\ &\quad - 4\epsilon(1 - \epsilon) \langle \psi | O \mathbb{E} [\langle \xi | \langle \xi |] O | \psi \rangle - 2\epsilon(1 - \epsilon) \langle \psi | O | \psi \rangle \text{Tr}[O \mathbb{E} |\xi\rangle \langle \xi|] \end{aligned} \quad (\text{C6})$$

$$\begin{aligned} &= (1 - \epsilon) \langle \psi | O^2 | \psi \rangle - (1 - \epsilon)^2 \langle \psi | O | \psi \rangle^2 + \epsilon \|O\|_F^2/d - \frac{4\epsilon(1 - \epsilon)}{d} \langle \psi | O^2 | \psi \rangle \\ &\quad - \epsilon^2 \frac{\text{Tr}[O]^2 + \|O\|_F^2}{d(d+1)} - \frac{2\epsilon(1 - \epsilon)}{d} \langle \psi | O | \psi \rangle \text{Tr}[O] \end{aligned} \quad (\text{C7})$$

$$= (1 - \epsilon) \langle \psi | O^2 | \psi \rangle - (1 - \epsilon)^2 \langle \psi | O | \psi \rangle^2 + \epsilon \|O\|_F^2/d - \frac{4\epsilon(1 - \epsilon)}{d} \langle \psi | O^2 | \psi \rangle - \frac{\epsilon^2}{d(d+1)} \|O\|_F^2. \quad (\text{C8})$$

Further note that for  $O$  being a Hamiltonian  $H$ , as similar but simpler calculation tells us how the expectation value is gradually shifted from  $E_i$  to average energy  $\bar{E}$ ,  $|\tilde{\psi}\rangle = \sqrt{1 - \epsilon} |E_i\rangle + \sqrt{\epsilon} |\xi\rangle$ :

$$\mathbb{E} [\langle \tilde{\psi} | H | \tilde{\psi} \rangle] = (1 - \epsilon) E_i + \epsilon \mathbb{E} [\langle \xi | H | \xi \rangle] = (1 - \epsilon) E_i + \epsilon \frac{1}{d} \text{Tr}(H) = (1 - \epsilon) E_i + \epsilon \bar{E} \quad (\text{C9})$$

Appendix D: 2D TFIM: Perturbative improvement estimations (Proof of Lemma 5)

1. "Disordered phase"  $h \gg J$

We normalize the Hamiltonian to obtain (this does not change the variance ratio):

$$H = -\sum_i X_i - \left(\frac{J}{h}\right) \sum_{\langle i,j \rangle} Z_i Z_j = -\sum_i X_i - \lambda \sum_{\langle i,j \rangle} Z_i Z_j = H_0 + \lambda V \quad (\text{D1})$$

The ground state  $|E_0\rangle$  is given up to second order in  $\lambda$  by:

$$|E_0^{(0)}\rangle = |+\rangle^{\otimes n} \quad (\text{D2})$$

$$|E_0^{(1)}\rangle = \sum_{|b\rangle \neq |+\rangle^{\otimes n}} \frac{\langle b | \sum_{\langle i,j \rangle} Z_i Z_j | + \rangle^{\otimes n}}{-n - (n-2 \cdot 2)} |b\rangle = \frac{1}{4} \sum_{\langle i,j \rangle} Z_i Z_j |+\rangle^{\otimes n} \quad (\text{D3})$$

$$|E_0^{(2)}\rangle = \sum_{|b_1\rangle \neq |+\rangle^{\otimes n}} \sum_{|b_2\rangle \neq |+\rangle^{\otimes n}} |b_1\rangle \frac{\langle b_1 | \sum_{\langle i,j \rangle} Z_i Z_j | b_2 \rangle \langle b_2 | \sum_{\langle i,j \rangle} Z_i Z_j | + \rangle^{\otimes n}}{\left(E_{|+\rangle^{\otimes n}}^{(0)} - E_{|b_1\rangle}^{(0)}\right) \left(E_{|+\rangle^{\otimes n}}^{(0)} - E_{|b_2\rangle}^{(0)}\right)} - \frac{1}{2} |+\rangle^{\otimes n} \frac{(2n)}{4^2} \quad (\text{D4})$$

$$= \left[ \frac{2}{4 \cdot 8} \sum_{\substack{\langle i,j \rangle, \langle k,\ell \rangle \\ i,j \neq k,\ell}} (Z_i Z_j)(Z_k Z_\ell) + \frac{4}{16} \sum_{\langle\langle i,j \rangle\rangle_{\text{diagonal}}} Z_i Z_j + \frac{2}{16} \sum_{\langle\langle i,j \rangle\rangle_{\text{axial}}} Z_i Z_j - \frac{n}{16} \mathbf{1} \right] |+\rangle^{\otimes n} \quad (\text{D5})$$

$$|E_0\rangle = \left[ \mathbf{1} + \frac{\lambda}{4} \sum_{\langle i,j \rangle} Z_i Z_j + \frac{\lambda^2}{16} \left( \sum_{\substack{\langle i,j \rangle, \langle k,\ell \rangle \\ i,j \neq k,\ell}} (Z_i Z_j)(Z_k Z_\ell) + 4 \sum_{\langle\langle i,j \rangle\rangle_{\text{diagonal}}} Z_i Z_j + 2 \sum_{\langle\langle i,j \rangle\rangle_{\text{axial}}} Z_i Z_j - n \mathbf{1} \right) \right] |+\rangle^{\otimes n} + \mathcal{O}(\lambda^3) \quad (\text{D6})$$

$$= P_X^{(2)} |+\rangle^{\otimes n} + \mathcal{O}(\lambda^3) \quad (\text{D7})$$

Note that  $\sum_{\langle\langle i,j \rangle\rangle_{\text{axial}}}$  obtains a factor 2 if  $n_x, n_y = 4$  and does not exist for  $n_x, n_y = 3$ . Let's start with calculating the variance of  $H_0$  up to second order

$$\text{Var}(H_0) = \langle (H_0)^2 \rangle - \langle H_0 \rangle^2 \quad (\text{D8})$$

$$\langle H_0 \rangle = \langle + |^{\otimes n} \left[ \mathbf{1} + \frac{\lambda}{4} \sum_{\langle i,j \rangle} Z_i Z_j + \frac{\lambda^2}{16} \left( \sum_{\substack{\langle i,j \rangle, \langle k,\ell \rangle \\ i,j \neq k,\ell}} (Z_i Z_j)(Z_k Z_\ell) + 4 \sum_{\langle\langle i,j \rangle\rangle_{\text{diagonal}}} Z_i Z_j + 2 \sum_{\langle\langle i,j \rangle\rangle_{\text{axial}}} Z_i Z_j - n \mathbf{1} \right) \right] \quad (\text{D9})$$

$$\sum_i X_i \left[ \mathbf{1} + \frac{\lambda}{4} \sum_{\langle i,j \rangle} Z_i Z_j + \frac{\lambda^2}{16} \left( \sum_{\substack{\langle i,j \rangle, \langle k,\ell \rangle \\ i,j \neq k,\ell}} (Z_i Z_j)(Z_k Z_\ell) + 4 \sum_{\langle\langle i,j \rangle\rangle_{\text{diagonal}}} Z_i Z_j + 2 \sum_{\langle\langle i,j \rangle\rangle_{\text{axial}}} Z_i Z_j - n \mathbf{1} \right) \right] |+\rangle^{\otimes n} + \mathcal{O}(\lambda^3) \quad (\text{D10})$$

$$= n + \lambda^2 \left( \frac{1}{4^2} (2n(n-2-2)) - 2 \frac{n^2}{16} \right) + \mathcal{O}(\lambda^3) = n - \frac{\lambda^2}{2} n + \mathcal{O}(\lambda^3) \quad (\text{D11})$$

$$\langle (H_0)^2 \rangle = \langle + |^{\otimes n} \left[ \mathbb{1} + \frac{\lambda}{4} \sum_{\langle i,j \rangle} Z_i Z_j + \frac{\lambda^2}{16} \left( \sum_{\substack{\langle i,j \rangle, \langle k,\ell \rangle \\ i,j \neq k,\ell}} (Z_i Z_j)(Z_k Z_\ell) + 4 \sum_{\substack{\langle \langle i,j \rangle \rangle \\ \text{diagonal}}} Z_i Z_j + 2 \sum_{\substack{\langle \langle i,j \rangle \rangle \\ \text{axial}}} Z_i Z_j - n \mathbb{1} \right) \right] \left[ n \mathbb{1} + \sum_{i \neq j} X_i X_j \right] \rangle \quad (\text{D12})$$

$$\left[ \mathbb{1} + \frac{\lambda}{4} \sum_{\langle i,j \rangle} Z_i Z_j + \frac{\lambda^2}{16} \left( \sum_{\substack{\langle i,j \rangle, \langle k,\ell \rangle \\ i,j \neq k,\ell}} (Z_i Z_j)(Z_k Z_\ell) + 4 \sum_{\substack{\langle \langle i,j \rangle \rangle \\ \text{diagonal}}} Z_i Z_j + 2 \sum_{\substack{\langle \langle i,j \rangle \rangle \\ \text{axial}}} Z_i Z_j - n \mathbb{1} \right) \right] |+\rangle^{\otimes n} + \mathcal{O}(\lambda^3) \quad (\text{D13})$$

$$= n^2 + \lambda^2 \left( \frac{2n[n + (n-2)(n-3)] + 2 - 4(n-2)}{16} - \frac{2n^3}{16} \right) + \mathcal{O}(\lambda^3) = n^2 + \frac{\lambda^2}{16} (-16n^2 + 32n) + \mathcal{O}(\lambda^3) \quad (\text{D14})$$

$$\text{Var}(H_0) = \langle (H_0)^2 \rangle - \langle H_0 \rangle^2 = n^2 + \lambda^2 (2n - n^2) - [n^2 - n^2 \lambda^2] + \mathcal{O}(\lambda^3) = 2n\lambda^2 + \mathcal{O}(\lambda^3) \quad (\text{D15})$$

Next lets calculate (For  $L > 1$ ):

$$\text{Var}(H_l - H_r) = \langle (H_l - H_r)^2 \rangle - \langle H_l - H_r \rangle^2 = 2 \langle (H_l)^2 \rangle - 2 \langle H_l H_r \rangle \quad (\text{D16})$$

$$H_l = \lambda \sum_{i=1}^{n_x/L} \sum_{j=1}^{n_y} Z_{Li,j} Z_{Li+1,j} \quad H_r = \lambda \sum_{i=1}^{n_x/L} \sum_{j=1}^{n_y} Z_{Li+1,j} Z_{Li+2,j} \quad (\text{D17})$$

This calculation is true also for  $L = 3$  as there the axial next nearest neighbors would be neighbours, but the term in the expansion does not exist then.

$$\langle \langle E_0 | H_l \rangle \langle H_l | E_0 \rangle \rangle = \quad (\text{D18})$$

$$\langle + |^{\otimes n} \left[ \mathbb{1} + \frac{\lambda}{4} \sum_{\langle i,j \rangle} Z_i Z_j + \frac{\lambda^2}{16} \left( \sum_{\substack{\langle i,j \rangle, \langle k,\ell \rangle \\ i,j \neq k,\ell}} (Z_i Z_j)(Z_k Z_\ell) + 4 \sum_{\substack{\langle \langle i,j \rangle \rangle \\ \text{diagonal}}} Z_i Z_j + 2 \sum_{\substack{\langle \langle i,j \rangle \rangle \\ \text{axial}}} Z_i Z_j - n \mathbb{1} \right) \right] \rangle \quad (\text{D19})$$

$$\lambda^2 \left[ \frac{n}{L} \mathbb{1} + \sum_{i=1}^{n_x/L} \sum_{j=1}^{n_y} \sum_{k=1}^{n_x/L} \sum_{\ell=1, (i,j) \neq (k,\ell)}^{n_y} Z_{Li,j} Z_{Li+1,j} Z_{Lk,\ell} Z_{Lk+1,\ell} \right] \quad (\text{D20})$$

$$\left[ \mathbb{1} + \frac{\lambda}{4} \sum_{\langle i,j \rangle} Z_i Z_j + \frac{\lambda^2}{16} \left( \sum_{\substack{\langle i,j \rangle, \langle k,\ell \rangle \\ i,j \neq k,\ell}} (Z_i Z_j)(Z_k Z_\ell) + 4 \sum_{\substack{\langle \langle i,j \rangle \rangle \\ \text{diagonal}}} Z_i Z_j + 2 \sum_{\substack{\langle \langle i,j \rangle \rangle \\ \text{axial}}} Z_i Z_j - n \mathbb{1} \right) \right] |+\rangle^{\otimes n} + \mathcal{O}(\lambda^3) \quad (\text{D21})$$

$$= \frac{n}{L} \lambda^2 + \frac{\lambda^4}{16} \left( \frac{n}{L} 2 \cdot 2n + 2 \cdot \frac{n}{L} \cdot \frac{n-1}{L} - 2 \cdot \frac{n^2}{L} + 2 \cdot 2 \cdot \frac{n}{L} \cdot \frac{n-1}{L} \right) + \mathcal{O}(\lambda^5) \quad (\text{D22})$$

$$= \frac{n}{L} \lambda^2 + \frac{\lambda^4 n^2}{16 L} \left( 4 + \frac{2}{L} - \frac{2}{nL} - 2 + \frac{4}{L} - \frac{4}{nL} \right) + \mathcal{O}(\lambda^5) = \frac{n}{L} \lambda^2 + \frac{\lambda^4 n^2}{16 L} \left( 2 + \frac{6}{L} \left( 1 - \frac{1}{n} \right) \right) + \mathcal{O}(\lambda^5) \quad (\text{D23})$$

$$\langle\langle E_0 | H_l \rangle\rangle \langle\langle H_r | E_0 \rangle\rangle = \quad (D24)$$

$$\langle + |^{\otimes n} \left[ \mathbb{1} + \frac{\lambda}{4} \sum_{\langle i,j \rangle} Z_i Z_j + \frac{\lambda^2}{16} \left( \sum_{\substack{\langle i,j \rangle, \langle k,\ell \rangle \\ i,j \neq k,\ell}} (Z_i Z_j)(Z_k Z_\ell) + 4 \sum_{\substack{\langle\langle i,j \rangle\rangle \\ \text{diagonal}}} Z_i Z_j + 2 \sum_{\substack{\langle\langle i,j \rangle\rangle \\ \text{axial}}} Z_i Z_j - n\mathbb{1} \right) \right] \quad (D25)$$

$$\left[ \lambda \sum_{i=1}^{n_x/L} \sum_{j=1}^{n_y} Z_{Li,j} Z_{L(i+1),j} \right] \left[ \lambda \sum_{i=1}^{n_x/L} \sum_{j=1}^{n_y} Z_{L(i+1),j} Z_{L(i+2),j} \right] \quad (D26)$$

$$\left[ \mathbb{1} + \frac{\lambda}{4} \sum_{\langle i,j \rangle} Z_i Z_j + \frac{\lambda^2}{16} \left( \sum_{\substack{\langle i,j \rangle, \langle k,\ell \rangle \\ i,j \neq k,\ell}} (Z_i Z_j)(Z_k Z_\ell) + 4 \sum_{\substack{\langle\langle i,j \rangle\rangle \\ \text{diagonal}}} Z_i Z_j + 2 \sum_{\substack{\langle\langle i,j \rangle\rangle \\ \text{axial}}} Z_i Z_j - n\mathbb{1} \right) \right] |+\rangle^{\otimes n} + \mathcal{O}(\lambda^3 \lambda^2) \quad (D27)$$

$$= \mathcal{O}(\lambda^4) \quad (D28)$$

Thus we have:

$$\text{Var}(H_0) = 2n\lambda^2 + \mathcal{O}(\lambda^3) \quad (D29)$$

$$\text{Var}(H_l - H_r) = 2 \cdot \frac{n}{L} \lambda^2 + \mathcal{O}(\lambda^4) \quad (D30)$$

$$\frac{\text{Var}(H_0)}{\text{Var}(\frac{1}{2}(H - H_l + H_r))} = 4 \frac{\text{Var}(H_1)}{\text{Var}(H_l - H_r)} = 4 \frac{2n\lambda^2}{2 \cdot \frac{n}{L} \lambda^2} + \mathcal{O}(\lambda) = 4L + \mathcal{O}(\lambda) \quad (D31)$$

## 2. "Ordered phase" $h \ll J$

We normalize the Hamiltonian to obtain (this does not change the variance ratio):

$$H = - \sum_{\langle i,j \rangle} Z_i Z_j - \left( \frac{h}{J} \right) \sum_i X_i = - \sum_{\langle i,j \rangle} Z_i Z_j - \lambda \sum_i X_i = H_0 + \lambda V \quad (D32)$$

Then we can calculate the perturbed state order by order:

$$\frac{\text{Var}(H_2)}{\text{Var}(\frac{1}{2}(H - H_l + H_r))} = 4 \frac{\text{Var}(H_1)}{\text{Var}(H_l - H_r)} \quad (D33)$$

We now want to calculate

$$|E_0^{(0)}\rangle = |0\rangle^{\otimes n} \quad (D34)$$

$$|E_0^{(1)}\rangle = \sum_{|b\rangle \neq |0\rangle^{\otimes n}} \frac{\langle b | \sum_i X_i | 0^{\otimes n} \rangle}{-2n - E_k^{(0)}} |b\rangle = \frac{1}{8} \sum_i X_i |0\rangle^{\otimes n} \quad (D35)$$

$$|E_0^{(2)}\rangle = \sum_{|b_1\rangle \neq |0\rangle^{\otimes n}} \sum_{|b_2\rangle \neq |0\rangle^{\otimes n}} |b_1\rangle \frac{\langle b_1 | \sum_i X_i | b_2 \rangle \langle b_2 | \sum_i X_i | 0^{\otimes n} \rangle}{(E_n^{(0)} - E_k^{(0)})(E_n^{(0)} - E_\ell^{(0)})} \quad (D36)$$

$$- \sum_{k \neq n} |k^{(0)}\rangle \frac{\langle k^{(0)} | V | n^{(0)} \rangle \langle 0^{\otimes n} | \sum_i X_i | 0^{\otimes n} \rangle}{(E_n^{(0)} - E_k^{(0)})^2} - \frac{1}{2} |0\rangle^{\otimes n} \frac{n}{8^2} \quad (D37)$$

$$= \left( \frac{2}{8 \cdot 2 \cdot 6} \sum_{\langle i,j \rangle} X_i X_j + \frac{1}{8 \cdot 2 \cdot 8} \sum_{i \neq j \setminus \langle i,j \rangle} X_i X_j - \frac{1}{128} n\mathbb{1} \right) |0\rangle^{\otimes n} \quad (D38)$$

$$|E_0\rangle = \left[ \mathbb{1} + \frac{\lambda}{8} \sum_i X_i + \frac{\lambda^2}{16} \left( \frac{1}{3} \sum_{\langle i,j \rangle} X_i X_j + \frac{1}{8} \sum_{i \neq j \setminus \langle i,j \rangle} X_i X_j - \frac{1}{8} n\mathbb{1} \right) \right] |0\rangle^{\otimes n} + \mathcal{O}(\lambda^3) \quad (D39)$$



Note here that the  $\sum_{\langle i,j \rangle}$  receives a factor 2 as then there is no double counting of lattice sides any more, while  $\sum_{i \neq j \setminus \langle i,j \rangle}$  still has every term twice.

Further note that we defined  $H_r = T_{-1}H_lT_1$ . In the  $L = 1$  case we use instead  $H_r = SH_lS$ . Further, we could have taken  $H_r = T_{-\lceil L/2 \rceil}H_lT_{\lceil L/2 \rceil}$ . Indeed, it turns out that the last definition performs a factor 2 worse than first one in the perturbative limit.

Let's start with calculating the variance of  $H_1 = \lambda \sum_i X_i$  up to second order

$$\text{Var}(H_1) = \langle (H_1)^2 \rangle - \langle H_1 \rangle^2 \quad (\text{D40})$$

$$\langle (H_1)^2 \rangle = \lambda^2 n + \lambda^2 \langle 0 |^{\otimes n} \left[ \mathbf{1} + \frac{\lambda}{8} \sum_i X_i + \frac{\lambda^2}{16} \left( \frac{1}{3} \sum_{\langle i,j \rangle} X_i X_j + \frac{1}{8} \sum_{i \neq j \setminus \langle i,j \rangle} X_i X_j - \frac{1}{8} n \mathbf{1} \right) \right] \left[ \sum_{i \neq j} X_i X_j \right] \quad (\text{D41})$$

$$\left[ \mathbf{1} + \frac{\lambda}{8} \sum_i X_i + \frac{\lambda^2}{16} \left( \frac{1}{3} \sum_{\langle i,j \rangle} X_i X_j + \frac{1}{8} \sum_{i \neq j \setminus \langle i,j \rangle} X_i X_j - \frac{1}{8} n \mathbf{1} \right) \right] |0\rangle^{\otimes n} + \mathcal{O}(\lambda^3 \lambda^2) \quad (\text{D42})$$

$$= \lambda^2 n + \lambda^4 \left( \frac{n \cdot 2(n-1)}{8^2} + 2 \frac{2n \cdot 2}{3 \cdot 16} + 2 \frac{[n(n-1) - 2n] \cdot 2}{8 \cdot 16} \right) + \mathcal{O}(\lambda^3 \lambda^2) \quad (\text{D43})$$

$$= \lambda^2 n + \lambda^4 \left( n^2 \left( \frac{1}{32} + \frac{1}{32} \right) + n \left( -\frac{1}{32} + \frac{1}{6} - \frac{3}{32} \right) \right) + \mathcal{O}(\lambda^5) = \lambda^2 n + \frac{\lambda^4}{16} \left( n^2 - \frac{4}{3} n \right) + \mathcal{O}(\lambda^5) \quad (\text{D44})$$

$$\langle H_1 \rangle = \lambda \langle 0 |^{\otimes n} \left[ \mathbf{1} + \frac{\lambda}{8} \sum_i X_i + \frac{\lambda^2}{16} \left( \frac{1}{3} \sum_{\langle i,j \rangle} X_i X_j + \frac{1}{8} \sum_{i \neq j \setminus \langle i,j \rangle} X_i X_j - \frac{1}{8} n \mathbf{1} \right) \right] \left[ \sum_i X_i \right] \quad (\text{D45})$$

$$\left[ \mathbf{1} + \frac{\lambda}{8} \sum_i X_i + \frac{\lambda^2}{16} \left( \frac{1}{3} \sum_{\langle i,j \rangle} X_i X_j + \frac{1}{8} \sum_{i \neq j \setminus \langle i,j \rangle} X_i X_j - \frac{1}{8} n \mathbf{1} \right) \right] |0\rangle^{\otimes n} + \mathcal{O}(\lambda^3 \lambda^1) \quad (\text{D46})$$

$$= \lambda^2 \left( \frac{2}{8} n \right) + \mathcal{O}(\lambda^4) \quad (\text{D47})$$

$$\text{Var}(H_1) = n \lambda^2 - \frac{1}{12} n \lambda^4 + \mathcal{O}(\lambda^5) \quad (\text{D48})$$

Let's calculate the variance of  $H_l - H_r$  up to second order. Let's consider a general  $H_r$  which is translated with respect to  $H_l$  by  $i_r \leq L/2$ .

$$\text{Var}\left(\frac{1}{2}(H - H_l + H_r)\right) = \frac{1}{4} \text{Var}(H_l - H_r) = \frac{1}{2} (\langle (H_l)^2 \rangle - \langle H_l H_r \rangle) \quad (\text{D49})$$

$$H_l = \sum_{i=1}^{n_x/L} \sum_{j=1}^{n_y} Z_{Li,j} Z_{L(i+1),j} \quad H_r = \sum_{i=1}^{n_x/L} \sum_{j=1}^{n_y} Z_{Li+i_r,j} Z_{L(i+i_r+1),j} \quad (\text{D50})$$

$$\langle (H_l)^2 \rangle = \frac{n}{L} + \langle 0 |^{\otimes n} \left[ \mathbf{1} + \frac{\lambda}{8} \sum_i X_i + \frac{\lambda^2}{16} \left( \frac{1}{3} \sum_{\langle i,j \rangle} X_i X_j + \frac{1}{8} \sum_{i \neq j \setminus \langle i,j \rangle} X_i X_j - \frac{1}{8} n \mathbf{1} \right) \right] \quad (\text{D51})$$

$$\left[ \sum_{i,k=1}^{n_x/L} \sum_{\substack{j,\ell=1 \\ (i,j) \neq (k,\ell)}}^{n_y} (Z_{Li,j} Z_{L(i+1),j}) (Z_{Lk,\ell} Z_{L(k+1),\ell}) \right] \quad (\text{D52})$$

$$\left[ \mathbf{1} + \frac{\lambda}{8} \sum_i X_i + \frac{\lambda^2}{16} \left( \frac{1}{3} \sum_{\langle i,j \rangle} X_i X_j + \frac{1}{8} \sum_{i \neq j \setminus \langle i,j \rangle} X_i X_j - \frac{1}{8} n \mathbf{1} \right) \right] |0\rangle^{\otimes n} + \mathcal{O}(\lambda^4) \quad (\text{D53})$$

$$= \left(\frac{n}{L}\right)^2 + \frac{\lambda^2}{64} \left(\frac{n}{L} \left(\frac{n}{L} - 1\right) (n - 2 \cdot 4) - 2 \frac{n}{2L} \left(\frac{n}{L} - 1\right)\right) + \mathcal{O}(\lambda^4) = \left(\frac{n}{L}\right)^2 - \frac{\lambda^2}{8} \frac{n}{L} \left(\frac{n}{L} - 1\right) + \mathcal{O}(\lambda^4) \quad (\text{D54})$$

$$\langle H_l H_r \rangle = \langle 0 |^{\otimes n} \left[ \mathbb{1} + \frac{\lambda}{8} \sum_i X_i + \frac{\lambda^2}{16} \left( \frac{1}{3} \sum_{\langle i,j \rangle} X_i X_j + \frac{1}{8} \sum_{i \neq j \setminus \langle i,j \rangle} X_i X_j - \frac{1}{8} n \mathbb{1} \right) \right] \quad (D55)$$

$$\left[ \delta_{L,2} \delta_{i_r,1} \sum_{i=1}^{n_x/L} \sum_{j=1}^{n_y} Z_{Li-1,j} Z_{Li+1,j} + \delta_{i_r,1} \sum_{i=1}^{n_x/L} \sum_{j=1}^{n_y} Z_{Li,j} Z_{Li+2,j} \right] \quad (D56)$$

$$+ \sum_{i,k=1}^{n_x/L} \sum_{\substack{j,\ell=1 \\ (Li,j) \neq (Lk+i_r, \{0\pm 1\}, \ell)}}^{n_y} (Z_{Li,j} Z_{Li+1,j}) (Z_{Lk+i_r,\ell} Z_{Lk+i_r+1,\ell}) \quad (D57)$$

$$\left[ \mathbb{1} + \frac{\lambda}{8} \sum_i X_i + \frac{\lambda^2}{16} \left( \frac{1}{3} \sum_{\langle i,j \rangle} X_i X_j + \frac{1}{8} \sum_{i \neq j \setminus \langle i,j \rangle} X_i X_j - \frac{1}{8} n \mathbb{1} \right) \right] |0\rangle^{\otimes n} + \mathcal{O}(\lambda^3) \quad (D58)$$

$$= \left( \frac{n}{L} \right)^2 + \frac{\lambda^2}{64} \left( (\delta_{L,2} + \delta_{i_r,1}) n \cdot \frac{n-2 \cdot 2}{L} + (n-2 \cdot 4) \frac{n}{L} \left( \frac{n}{L} - \delta_{L,2} - \delta_{i_r,1} \right) - 2 \frac{n^3}{2L^2} \right) + \mathcal{O}(\lambda^4) \quad (D59)$$

$$= \left( \frac{n}{L} \right)^2 + \frac{\lambda^2}{16} \frac{n^2}{L} \left( \left( \frac{n-8}{L} + (\delta_{L,2} + \delta_{i_r,1}) \frac{4}{n} \right) - \frac{n}{4L} \right) + \mathcal{O}(\lambda^4) \quad (D60)$$

note that  $L = 2$  implies  $i_r = 1$ . We have  $\mathcal{O}(\lambda^4)$ , not only  $\mathcal{O}(\lambda^3)$  as the third perturbation order contains single and triple excitations and thus the product of zeroth and third order terms vanish as well. The third sum has  $\frac{n^2}{L^2} - (\delta_{L,2} + \delta_{i_r,1}) \frac{n}{L}$  elements. Whenever  $XZX$  act on the same qubits, we obtain  $-Z$  and we obtain  $+Z$  if they act on different qubits. For  $L = 2$ , we have

$$H_l = \sum_{i=1}^{n_x/L} \sum_{j=1}^{n_y} Z_{2i,j} Z_{2i+1,j} \quad H_r = \sum_{i=1}^{n_x/L} \sum_{j=1}^{n_y} Z_{2i+1,j} Z_{2i+2,j} \quad (D61)$$

$$H_l H_r = \sum_{i=1}^{n_x/L} \sum_{j=1}^{n_y} \sum_{k=1}^{n_x/L} \sum_{l=1}^{n_y} Z_{2i,j} Z_{2i+1,j} Z_{2k+1,l} Z_{2k+2,l} \quad (D62)$$

So

$$\langle H_l H_r \rangle = \langle 0 |^{\otimes n} \left[ \mathbb{1} + \frac{\lambda}{8} \sum_i X_i + \frac{\lambda^2}{16} \left( \frac{1}{3} \sum_{\langle i,j \rangle} X_i X_j + \frac{1}{8} \sum_{i \neq j \setminus \langle i,j \rangle} X_i X_j - \frac{1}{8} n \mathbb{1} \right) \right] \quad (D63)$$

$$\sum_{i=1}^{n_x/L} \sum_{j=1}^{n_y} \sum_{k=1}^{n_x/L} \sum_{l=1}^{n_y} Z_{2i,j} Z_{2i+1,j} Z_{2k+1,l} Z_{2k+2,l} \quad (D64)$$

$$\left[ \mathbb{1} + \frac{\lambda}{8} \sum_i X_i + \frac{\lambda^2}{16} \left( \frac{1}{3} \sum_{\langle i,j \rangle} X_i X_j + \frac{1}{8} \sum_{i \neq j \setminus \langle i,j \rangle} X_i X_j - \frac{1}{8} n \mathbb{1} \right) \right] |0\rangle^{\otimes n} + \mathcal{O}(\lambda^3) \quad (D65)$$

$$= \left( \frac{n}{L} \right)^2 + \frac{\lambda^2}{64} \left( 2 \frac{n}{L} (n-4) + \left( \left( \frac{n}{L} \right)^2 - 2 \frac{n}{L} \right) (n-8) - \frac{n^3}{L^2} \right) + \mathcal{O}(\lambda^4) \quad (D66)$$

$$= \left( \frac{n}{L} \right)^2 + \frac{\lambda^2}{8} \frac{n}{L} \left( 1 - \frac{n}{L} \right) + \mathcal{O}(\lambda^4) \quad (D67)$$

Together, this gives:

$$\langle (H_l)^2 \rangle - \langle H_l H_r \rangle = \lambda^2 \left( -\frac{1}{8} \frac{n}{L} \left( \frac{n}{L} - 1 \right) + \frac{1}{8} \frac{n}{L} \left( \frac{n}{L} - 1 \right) \right) + \mathcal{O}(\lambda^4) = \mathcal{O}(\lambda^4) \quad (D68)$$

For  $L > 2$  we have:

$$\langle H_l H_r \rangle = \langle 0 |^{\otimes n} \left[ \mathbf{1} + \frac{\lambda}{8} \sum_i X_i + \frac{\lambda^2}{16} \left( \frac{1}{3} \sum_{\langle i,j \rangle} X_i X_j + \frac{1}{8} \sum_{i \neq j \setminus \langle i,j \rangle} X_i X_j - \frac{1}{8} n \mathbf{1} \right) \right] \rangle \quad (\text{D69})$$

$$\sum_{i=1}^{n_x/L} \sum_{j=1}^{n_y} \sum_{k=1}^{n_x/L} \sum_{l=1}^{n_y} Z_{Li,j} Z_{Li+1,j} Z_{Lk+1,l} Z_{Lk+2,l} \quad (\text{D70})$$

$$\left[ \mathbf{1} + \frac{\lambda}{8} \sum_i X_i + \frac{\lambda^2}{16} \left( \frac{1}{3} \sum_{\langle i,j \rangle} X_i X_j + \frac{1}{8} \sum_{i \neq j \setminus \langle i,j \rangle} X_i X_j - \frac{1}{8} n \mathbf{1} \right) \right] |0\rangle^{\otimes n} + \mathcal{O}(\lambda^3) \quad (\text{D71})$$

$$= \left( \frac{n}{L} \right)^2 + \frac{\lambda^2}{64} \left( \left( \frac{n}{L} \right) (n-4) + \left( \left( \frac{n}{L} \right)^2 - \frac{n}{L} \right) (n-8) - \frac{n^3}{L^2} \right) + \mathcal{O}(\lambda^4) \quad (\text{D72})$$

$$= \left( \frac{n}{L} \right)^2 - \frac{\lambda^2}{8} \left( \left( \frac{n}{L} \right)^2 - \frac{1}{2} \frac{n}{L} \right) + \mathcal{O}(\lambda^4) \quad (\text{D73})$$

Together, this gives:

$$\langle (H_l)^2 \rangle - \langle H_l H_r \rangle = \frac{\lambda^2}{8} \left( -\frac{n}{L} \left( \frac{n}{L} - 1 \right) + \left( \frac{n}{L} \right)^2 - \frac{1}{2} \frac{n}{L} \right) + \mathcal{O}(\lambda^4) = \frac{\lambda^2}{16} \frac{n}{L} + \mathcal{O}(\lambda^4) \quad (\text{D74})$$

Finally

$$\frac{\text{Var}(H_2)}{\text{Var}(\frac{1}{2}(H - H_l + H_r))} = 32L + \mathcal{O}(\lambda^2) \quad (\text{D75})$$

For  $L > 2$  und  $1 < i_r \leq L/2$

$$\langle H_l H_r \rangle = \langle 0 |^{\otimes n} \left[ \mathbf{1} + \frac{\lambda}{8} \sum_i X_i + \frac{\lambda^2}{16} \left( \frac{1}{3} \sum_{\langle i,j \rangle} X_i X_j + \frac{1}{8} \sum_{i \neq j \setminus \langle i,j \rangle} X_i X_j - \frac{1}{8} n \mathbf{1} \right) \right] \rangle \quad (\text{D76})$$

$$\sum_{i=1}^{n_x/L} \sum_{j=1}^{n_y} \sum_{k=1}^{n_x/L} \sum_{l=1}^{n_y} Z_{Li,j} Z_{Li+1,j} Z_{Lk+i_r,l} Z_{Lk+i_r+1,l} \quad (\text{D77})$$

$$\left[ \mathbf{1} + \frac{\lambda}{8} \sum_i X_i + \frac{\lambda^2}{16} \left( \frac{1}{3} \sum_{\langle i,j \rangle} X_i X_j + \frac{1}{8} \sum_{i \neq j \setminus \langle i,j \rangle} X_i X_j - \frac{1}{8} n \mathbf{1} \right) \right] |0\rangle^{\otimes n} + \mathcal{O}(\lambda^3) \quad (\text{D78})$$

$$= \left( \frac{n}{L} \right)^2 + \frac{\lambda^2}{64} \left( \left( \frac{n}{L} \right)^2 (n-8) - \frac{n^3}{L^2} \right) + \mathcal{O}(\lambda^4) = \left( \frac{n}{L} \right)^2 - \frac{\lambda^2}{8} \left( \frac{n}{L} \right)^2 + \mathcal{O}(\lambda^4) \quad (\text{D79})$$

Together, this gives:

$$\langle (H_l)^2 \rangle - \langle H_l H_r \rangle = \frac{\lambda^2}{8} \left( -\frac{n}{L} \left( \frac{n}{L} - 1 \right) + \left( \frac{n}{L} \right)^2 \right) + \mathcal{O}(\lambda^4) = \frac{\lambda^2}{8} \frac{n}{L} + \mathcal{O}(\lambda^4) \quad (\text{D80})$$

Finally

$$\frac{\text{Var}(H_2)}{\text{Var}(\frac{1}{2}(H - H_l + H_r))} = 16L + \mathcal{O}(\lambda^2) \quad (\text{D81})$$

For  $L = 1$  we need to define:

$$H_l = \sum_{i=1}^{n_x} \sum_{j=1}^{n_y} Z_{i,j} Z_{i+1,j} \quad H_r = S H_l S = \sum_{i=1}^{n_x} \sum_{j=1}^{n_y} Z_{i,j} Z_{i,j+1} \quad (\text{D82})$$

$$H_l H_r = \sum_{i=1}^{n_x} \sum_{j=1}^{n_y} \sum_{k=1}^{n_x} \sum_{l=1}^{n_y} Z_{i,j} Z_{i+1,j} Z_{k,l} Z_{k+1,l} \quad (\text{D83})$$

$$\langle H_l H_r \rangle = \langle 0 |^{\otimes n} \left[ \mathbf{1} + \frac{\lambda}{8} \sum_i X_i + \frac{\lambda^2}{16} \left( \frac{1}{3} \sum_{\langle i,j \rangle} X_i X_j + \frac{1}{8} \sum_{i \neq j \setminus \langle i,j \rangle} X_i X_j - \frac{1}{8} n \mathbf{1} \right) \right] \rangle \quad (\text{D84})$$

$$\sum_{i=1}^{n_x} \sum_{j=1}^{n_y} \sum_{k=1}^{n_x} \sum_{l=1}^{n_y} Z_{i,j} Z_{i+1,j} Z_{k,l} Z_{k+1,l} \quad (\text{D85})$$

$$\left[ \mathbf{1} + \frac{\lambda}{8} \sum_i X_i + \frac{\lambda^2}{16} \left( \frac{1}{3} \sum_{\langle i,j \rangle} X_i X_j + \frac{1}{8} \sum_{i \neq j \setminus \langle i,j \rangle} X_i X_j - \frac{1}{8} n \mathbf{1} \right) \right] |0\rangle^{\otimes n} + \mathcal{O}(\lambda^3) \quad (\text{D86})$$

$$= n^2 + \frac{\lambda^2}{64} (2n(n-4) + ((n^2 - 2n)(n-8) - n^3)) + \mathcal{O}(\lambda^4) \quad (\text{D87})$$

$$= n^2 + \frac{\lambda^2}{8} n(1-n) + \mathcal{O}(\lambda^4) \quad (\text{D88})$$

Thus:

$$(\langle (H_l)^2 \rangle - \langle H_l H_r \rangle) = \lambda^2 \left( -\frac{n}{8} (n-1) + \frac{n}{8} (n-1) \right) + \mathcal{O}(\lambda^4) = \mathcal{O}(\lambda^4) \quad (\text{D89})$$